Comparing orbiter and rover image-based mapping of an ancient sedimentary environment, Aeolis Palus, Gale crater, Mars

K.M. Stack, C.S. Edwards, J.P. Grotzinger, S. Gupta, D.Y. Sumner, F.J. Calef, L.A. Edgar, K.S. Edgett, A.A. Fraeman, S.R. Jacob, et al.

Comparing orbiter and rover image-based mapping of an ancient sedimentary environment, Aeolis Palus, Gale crater, Mars

K. M. Stack[1], C. S. Edwards[2], J. P. Grotzinger[3], S. Gupta[4], D. Y. Sumner[5], F. J. Calef, III[1], L.A. Edgar[2], K. S. Edgett[6], A. A. Fraeman[3], S. R. Jacob[7], L. Le Deit[8], K. W. Lewis[9], M. S. Rice[10], D. Rubin[11], R. M. E. Williams[12], K. H. Williford[1]

[1]*Jet Propulsion Laboratory, California Institute of Technology, Pasadena, CA 91109, USA*
[2]*Astrogeology Science Center, United States Geological Survey, Flagstaff, AZ 86001, USA*
[3]*Department of Geological and Planetary Sciences, California Institute of Technology, Pasadena, CA 91125, USA*
[4]*Department of Earth Science and Engineering, Imperial College, London, SW7 2AZ, UK*
[5]*Department of Earth and Planetary Sciences, University of California Davis, Davis, CA 95616, USA*
[6]*Malin Space Science Systems, Inc., San Diego, CA 92191-0148, USA*
[7]*Department of Geology and Geophysics, University of Hawai'I at Manoa, Honolulu, HI 96822, USA*
[8]*Laboratoire de Planétologie et Géodynamique de Nantes, Université de Nantes, Nantes, France*
[9]*Department of Earth and Planetary Sciences, Johns Hopkins University, Baltimore, MD, 21218, USA*
[10]*Department of Physics and Astronomy, Western Washington University, Bellingham, WA 98225, USA*
[11]*Department of Earth and Planetary Sciences, UC Santa Cruz, Santa Cruz, CA 95064, USA*
[12]*Planetary Science Institute, Tucson, AZ 85719, USA.*

Email address: kathryn.m.stack@jpl.nasa.gov

Keywords: Mars; Mars, surface; Geological Processes

Highlights

- Orbital facies were mapped at the Darwin, Cooperstown, and Kimberley waypoints in Gale crater.
- Orbital maps were compared with image-based observations from the Curiosity rover.
- Integrated orbital and rover observations are necessary to construct high fidelity depositional models.

Abstract

The Mars Science Laboratory team selected several waypoints along the ~10 km traverse across the Bradbury Rise area of Aeolis Palus from Yellowknife Bay to the base of Aeolis Mons for detailed analysis with the integrated Curiosity rover payload. These waypoints, informally named Darwin, Cooperstown, and Kimberley, were selected in orbital images because they contained outcrops hypothesized to provide exposures of Aeolis Palus stratigraphy. In this study, geologic maps were constructed for each waypoint using grayscale and color images from the High Resolution Imaging Science Experiment (HiRISE) camera onboard the Mars Reconnaissance Orbiter (MRO). Orbital facies were distinguished at each waypoint based on the relative brightness, color hue, and texture of the surface visible in HiRISE images and compared with Curiosity rover observations made using context mosaics from the 100 mm focal length Mast Camera (Mastcam) and images from the Mars Hand Lens Imager (MAHLI). Orbital facies mapped at Darwin, Cooperstown, and Kimberley were identified with rover observations as fine to coarse-grained cross-bedded sandstones and pebble conglomerates interpreted to represent

fluvial deposition. The Kimberley waypoint includes an orbital facies characterized by northwest-oriented striations in map view. In situ observations of this orbital facies show it to be composed of generally southward-dipping sandstone beds. This study presents an analysis and comparison of mapped orbital facies at the three waypoints, showing how orbiter and rover data can be integrated and compared to test the validity of orbital versus ground-based stratigraphic correlations within Gale crater. This study finds that fine-scale orbital geologic mapping of current and future Mars landing is essential for planning rover science investigations as well as predicting in advance the diversity of rock outcrops and deposits a rover can expect to encounter on the surface.

1. Introduction

Geologic maps provide a two-dimensional representation at the surface of the three-dimensional spatial and temporal relationships of lithologic or chronostratigraphic units that make up a planet's crust. For planets and other solar system bodies whose surfaces can only be studied remotely via telescopic, flyby, orbital, airborne, lander, or rover observations, photogeologic mapping is an important tool for providing insight into the geometric disposition of geologic units and the evolution of planetary surfaces. Despite the increased sophistication and spatial resolution of recent orbiter image-based geologic mapping efforts, considerable uncertainties remain in the manners in which investigators gather their observations and interpret orbiter image data [*Wilhelms*, 1990; *Hansen*, 2000; *Tanaka et al.*, 2009].

Independent ground truth of orbital geological interpretations is currently impossible for most of the martian surface, but such comparisons can be made for the seven locations that have been visited by rovers or landers; Chryse Planitia (Viking 1), Utopia Planitia (Viking 2), Ares

47 Vallis (Mars Pathfinder), Meridiani Planum and Gusev crater (Mars Exploration Rover (MER)
48 mission Opportunity and Spirit rovers, respectively), Vastitas Borealis (Phoenix Mars lander),
49 and Gale crater (Mars Science Laboratory (MSL) Curiosity rover). Orbiter and rover or lander
50 image-based comparisons can provide important insights into the fidelity of paleoenvironmental
51 interpretations made with these datasets by establishing a connection between "mega-scale"
52 orbital observations and those made on-site at the rover "macro- to micro-scale." Understanding
53 the value-added nature of geologic investigations using multiple spatial scales is particularly
54 important for currently active rover missions like MSL and MER Opportunity which rely heavily
55 on orbital geologic interpretations to assist in scientific traverse planning [*Grotzinger et al.*,
56 2014; *Arvidson et al.*, 2014; *Arvidson et al.*, 2015; *Crumpler et al.*, 2011, 2015]. Future missions
57 like InSight, the European Space Agency (ESA) ExoMars 2018 rover, and the Mars2020 rover
58 will also use orbital image datasets and geologic interpretations of these datasets to guide landing
59 site selection. Orbiter and rover image-based comparisons can also be used to extend geologic
60 interpretations made from orbital data, particularly those regarding paleoenvironment and past
61 conditions for habitability, to elsewhere on the planet where ground-truth observations are
62 unlikely to be available.
63 Gale crater, landing site of the MSL Curiosity rover (Figure 1), provides an ideal place
64 for such a comparison given the variety of scales at which this location has been mapped from
65 images acquired from orbit [*Malin and Edgett*, 2000; *Anderson and Bell*, 2010; *Milliken et al.*,
66 2010; *Thomson et al.*, 2011; *LeDeit et al.*, 2013; *Calef et al.*, 2013; *Rice et al.*, 2013b; *Grotzinger*
67 *et al.*, 2014, this study] and the sequence of sedimentary rocks present in Gale crater now known
68 to represent conditions favorable for past habitability [*Grotzinger et al.*, 2014]. This study
69 presents geologic maps constructed from High Resolution Imaging Science Experiment

(HIRISE) images, henceforth referred to as orbital geologic maps, and interpreted cross-sections produced at a scale of 1:500 from HiRISE images and digital terrain models (DTMs) for three major Curiosity rover field investigation sites, waypoints informally named Darwin, Cooperstown and Kimberley. The rover team analyzed these waypoints during Curiosity's ~10 km traverse across Bradbury Rise from Yellowknife Bay to the base of Aeolis Mons [*Vasavada et al*., 2014] (Figure 2). The orbital geologic maps and cross-sections presented here, which represent the most detailed observations and interpretations based on orbital images of these areas to-date, are then compared to Curiosity rover Mast Camera (Mastcam) and Mars Hand Lens Imager (MAHLI) observations of bedrock outcrop and unconsolidated surficial deposits at each waypoint. In addition to providing general comparisons of orbiter and rover image-based geologic observations and interpretations at each waypoint, this study presents a critical examination of the validity and significance of geologic mapping and stratigraphic interpretations made using remotely acquired orbiter image datasets. Conclusions are drawn about the past depositional settings and paleoenvironments present in Gale crater using correlations between rover and orbiter image data.

2. Background

Flyby and orbiter images of the martian surface acquired during the 1960s and 1970s by the Mariner and Viking spacecraft enabled the creation of increasingly detailed and comprehensive geologic maps, such as those by *Scott and Carr* [1978], *Scott and Tanaka* [1986], *Greeley and Guest* [1987], and *Tanaka and Scott* [1987]. Geologic maps based on Mariner 9 and Viking data remained state-of-the-art until the early 2000s when a series of high-resolution orbital imaging systems onboard Mars Global Surveyor (MGS), Mars Odyssey, Mars Express,

93 and the Mars Reconnaissance Orbiter (MRO) acquired thermal, visible, and near-infrared images
94 of the martian surface that have enabled detailed local and regional geologic mapping efforts
95 down to the sub-meter scale (e.g., *Rice et al.* [2013a], *Okubo* [2014], and *Sun and Milliken*
96 [2014], among many others). Analysis of these recent datasets has also led to refinements and
97 updates to a global geologic map of Mars [*Tanaka et al.*, 2014].
98 The Viking 1 and 2 landers afforded the first opportunity to ground-truth orbital geologic
99 map interpretations of Mars [*Binder et al.*, 1977; *Jakosky and Christensen*, 1986; *Crumpler et*
100 *al*., 2001; *Thomson and Schultz*, 2007]. Nearly twenty years later came confirmation of orbital
101 interpretations at the Ares Vallis landing site for the Pathfinder mission [*Komatsu and Baker*,
102 1997; *Rice and Edgett*, 1997, *Smith et al.*, 1997]. The landing site selection process for the MER
103 Spirit and Opportunity was the first to take advantage of meter-scale high-resolution image data
104 provided by MGS and Mars Odyssey [*Golombek et al.*, 2003]. Subsequent to landing, *Golombek*
105 *et al.* [2005] and [2006] addressed inconsistencies between orbital geologic interpretations and
106 observations of in situ geochemistry and depositional environments observed with the MER
107 Opportunity and Spirit rovers. Beginning in late 2006, Spirit and Opportunity surface science
108 operations also made use of images from the HiRISE camera onboard MRO as a tool for
109 geologic interpretation and mission planning [*Arvidson et al.*, 2006; *Golombek et al.*, 2006; *Wray*
110 *et al.*, 2009; *Wiseman et al.*, 2010; *Crumpler et al*., 2011, 2015; *Arvidson et al.*, 2015]. The
111 Phoenix Lander mission which launched in 2007 also made use of HIRISE images during the
112 selection and hazard evaluation of its landing site in the northern plains of Mars [*Arvidson et al.*,
113 2008; *Golombek et al.*, 2008; *Seelos et al.*, 2008]. The MSL mission is the first rover mission to
114 use HiRISE orbital images during the landing site selection process [*Anderson and Bell,* 2010;
115 *Golombek et al.*, 2012; *Grotiznger et al., 2012; Rice et al.*, 2013a], and orbital geologic mapping

116 of the Gale crater ellipse has provided critical context for Curiosity rover observations since
117 landing [*Calef et al*., 2013; *Rice et al.*, 2013b; *Grotzinger et al.*, 2014; *Arvidson et al.*, 2014].
118
119 **2.1. Previous Orbital Geologic Mapping of MSL Curiosity Landing Ellipse**
120 The main focus of previous mapping studies has been on the strata of Aeolis Mons, the
121 ~5 km-thick mound in the center of the crater [*Malin and Edgett*, 2000; *Milliken et al.*, 2010;
122 *Thomson et al.*, 2011]. Prior to Curiosity's landing in Gale crater, only *Anderson and Bell* [2010]
123 published a geologic map of the MSL landing ellipse, a 20 km by 7 km ellipse positioned on
124 Aeolis Palus, the plains surrounding Aeolis Mons. Since landing, *Le Deit et al.* [2013], *Calef et*
125 *al.* [2013], *Rice et al.*, [2013b], *Sumner et al.*, 2013, and *Grotzinger et al.* [2014] have mapped
126 some or all of the area covered by the MSL landing ellipse at varying scales and levels of detail.
127 *Anderson and Bell* [2010] mapped the area covered by the MSL landing ellipse, including
128 the three areas explored in this study, using MRO Context Camera (CTX) images (6 m/pixel).
129 Although the map scale was not explicitly stated in the study, they mapped at a relatively coarse
130 scale with a focus on geological and stratigraphic relationships on the scale of hundreds of
131 meters to kilometers. Over the area of Aeolis Palus traversed by the Curiosity rover, *Anderson*
132 *and Bell* [2010] mapped two geomorphic units: a hummocky plains unit and a mound-skirting
133 unit. The three areas examined in this study were mapped as part of the hummocky plains unit.
134 The hummocky plains unit was described as "hummocky terrain of smoothly-varying thermal
135 inertia" with a fairly uniform albedo in CTX images and was interpreted by *Anderson and Bell*
136 [2010] to represent largely unconsolidated material transitioning to fractured bedrock. Sinuous
137 ridges locally found on this unit were interpreted as inverted fluvial channels, but no other
138 indicators of geologic process were described. The mound-skirting unit, which was interpreted to

139 be younger than the hummocky plains unit, was described as an erosion-resistant, mesa-forming
140 geologic unit, the surface of which shows many small pits and ridges interpreted to be largely
141 fluvial and eolian in origin.

142 *Le Deit et al.* [2013] produced a geologic map of the entire interior of Gale crater using
143 Mars Express High Resolution Stereo Camera (HRSC), CTX, and HiRISE images and HRSC
144 DTMs to construct cross-sections across large swaths of the crater interior. They distinguished
145 several "crater floor" units, although all of the Aeolis Palus terrain traversed by the Curiosity
146 rover was mapped as a single crater floor unit (Cf1). The Cf1 unit extends from the northern
147 crater rim to the base of Aeolis Mons and was interpreted to represent fluvial, alluvial, and
148 colluvial deposition in a bajada complex located downstream from valleys incised into the
149 northern rim of Gale crater. The Cf1 unit was interpreted to be younger than the lowest strata of
150 Aeolis Mons, but likely older than most of the upper mound strata.

151 A detailed mapping effort focused on the MSL landing ellipse was presented in
152 *Grotzinger et al.* [2014], summarizing the preliminary efforts of *Calef et al.* [2013], *Rice et al.*
153 [2013b], and *Sumner et al.* [2013] (Figure 3). Prior to Curiosity's landing, the MSL science team
154 undertook a geologic mapping effort using HiRISE images and DTMs derived from HiRISE
155 stereo via the methods of *Kirk et al.* [2008]. The main objective of this mapping effort was to
156 guide initial traverse planning after the rover touched down and the location was known. The
157 map would also provide context and guidance for subsequent traverse and science investigation
158 planning. Through this effort, the landing ellipse was subdivided into six geologic units: Alluvial
159 Fan (AF), Bedded Fractured (BF), Cratered Surface (CS), Hummocky Plains (HP), Rugged
160 (RT), and Striated (SR). The Curiosity rover encountered the BF unit in the lower strata exposed
161 in Yellowknife Bay [*Grotzinger et al.*, 2014; *Arvidson et al.*, 2014], but the terrain across which

the rover traversed to the base of Mount Sharp was mapped primarily as consisting of units HP and RT, with intermittent exposures of CS and SR [*Calef et al.*, 2013; *Rice et al.*, 2013b; *Arvidson et al.*, 2014; *Grotzinger et al.*, 2014; *Vasavada et al.*, 2014]. The HP unit exhibits low surface roughness, uniform tone, and decimeter-scale topographic hummocks [*Calef et al.*, 2013; *Rice et al.*, 2013b; *Grotzinger et al.*, 2014] and corresponds generally to *Anderson and Bell's* [2010] hummocky plains unit. The RT unit was identified in HiRISE images as isolated exposures throughout the first third of the traverse to Aeolis Mons, although larger (100s m^2), more continuous exposures of RT were mapped in the southern part of the landing ellipse. The RT is characterized by its brightness relative to surroundings, topographic variability, meter to decameter-scale surface roughness, and contains erosion-resistant scarps [*Calef et al.*, 2013; *Rice et al.*, 2013b; *Grotzinger et al.*, 2014]. The CS unit is characterized by sub-planar surfaces containing a relatively high density of sub-kilometer diameter impact craters that occur at different elevations throughout the landing ellipse [*Calef et al.*, 2013; *Rice et al.*, 2013b; *Grotzinger et al.*, 2014*; Jacob et al.*, submitted]. The RT and CS units described in *Grotzinger et al.* [2014], though mapped in greater detail, correspond generally to the mound-skirting unit of *Anderson and Bell* [2010]. Exposures of the SR unit occur exclusively in the south central portion of the landing ellipse, and consist of isolated light-toned outcrops exhibiting a distinct northeast-southwest trending lineation visible in high-resolution orbital images. Relative age relationships between the HP, RT, CS, and SR unit are often ambiguous, and *Rice et al.* [2013b] acknowledged that these units, particularly the RT and CS units, may represent distinct textural or geomorphic surface expressions rather than stratigraphic units that can be projected into the subsurface.

185 **2.2. Curiosity's Traverse of Bradbury Rise**

186 Upon landing on Aeolis Palus in August of 2012, the MSL Curiosity rover traversed east
187 from Bradbury landing to an embayment of rock outcrop called Yellowknife Bay [*Grotzinger et*
188 *al.*, 2014] (Figure 2). Before Curiosity's departure from Yellowknife Bay toward the base of
189 Aeolis Mons in July of 2013, the MSL team selected several waypoints along the planned
190 traverse path across Bradbury Rise, a topographic high that extends north several kilometers
191 from the base of Aeolis Mons to the distal end of present-day Peace Vallis fan [*Vasavada et al.*,
192 2014; *Arvidson et al.*, 2014] (Figures 1 and 2). These three waypoints: Darwin, Cooperstown,
193 and Kimberley, were selected at approximately equidistant spacing along the planned route using
194 HiRISE images and the orbital geologic map of *Calef et al.* [2013] [*Vasavada et al.*, 2014]
195 (Figure 2a, Table 1). The Darwin site was chosen because of the presence of a conspicuous
196 ~200 m sub-circular outcrop of bright bedrock amid the hummocky plains of Bradbury Rise
197 (Figure 2b). Similar isolated occurrences of bright bedrock were observed in HiRISE images
198 throughout Bradbury Rise, and the Darwin waypoint was chosen as a representative of these
199 outcrops [*Vasavada et al.*, 2014]. The Cooperstown area (Figure 2c) was selected for study based
200 on the presence of a variety of bright bedrock outcrops observed in HiRISE images, some of
201 which exhibited meter-scale polygonal forms bounded by fractures that appeared similar in the
202 HiRISE images to fracture-delineated polygonal forms in the fine-grained sedimentary rocks
203 observed at Yellowknife Bay. These waypoints served as intermediate stops between
204 Yellowknife Bay and the third waypoint, Kimberley (Figure 2d). The Kimberley area attracted
205 interest early in the mission due to the presence in HiRISE images of a layered stratigraphy
206 expressed by differential erosion of the terrain. Some outcrop exposures in this area of the ellipse
207 contained striations, regularly spaced linear features extending ~tens of meters in length, that

were particularly distinct from other outcrops observed in the landing ellipse region [*Calef et al.*, 2013; *Rice et al.*, 2013b; *Grotzinger et al.*, 2014]. It was anticipated that an imaging and geochemical analysis campaign would help determine the origin of the striated outcrops, as well as their relationship with the nearby hummocky terrain and overlying bedded rocks [*Vasavada et al*., 2014].

The MSL team also acquired opportunistic remote sensing and contact science observations of float rocks, outcrops, eolian deposits, and regolith in between each of the three waypoints described above. However, the orbiter and rover image-based observations at Darwin, Cooperstown, and Kimberley are broadly representative of the geology observed during the traverse across Bradbury Rise (Figures 4-10), and also provide the best opportunities for direct comparison due to the exposures of bedrock and surficial deposits that can be resolved and distinguished in HiRISE images.

3. Data and Methods

3.1 Orbital Geologic Mapping

Maps based on planetary orbital image datasets most commonly use the terms "geologic unit" or "geomorphic unit" to refer to the two-dimensional surface areas bounded by drawn contacts. These terms are sometimes used interchangeably in planetary mapping, although conventional planetary mapping guidelines offer clear distinctions. According to Wilhelms [1990], a geologic unit is distinguished in planetary image data by its topographic expression and remotely observed surface properties, and refers to a "sheetlike, wedgelike, or tabular body of rock that underlies the surface…and not a surface, a geomorphic terrain, or a group of landforms." As part of the most recent global geologic mapping effort for Mars, *Tanaka et al.*

231 [2014] define geologic map units as "temporally unique geologic materials of substantial
232 thickness and extent for portrayal at map scale," and use primary formational morphology,
233 brightness and/or albedo, and spatial, stratigraphic, and relative crater age relationships to
234 delineate units. Materials interpreted to be surficial in nature or features interpreted to be the
235 result of secondary modification processes are not mapped as units.

236 Others prefer the term "geomorphic unit" in a planetary mapping context (e.g., *Anderson*
237 *and Bell* [2010], *Sun and Milliken* [2014]). Use of the term "geomorphic unit" generally avoids
238 the three-dimensional geometrical interpretation, implicit assumption of "rock" (as opposed to
239 unconsolidated surface materials), interpretation of primary formational versus secondary
240 modification features, temporal implications, or other exclusions implied by the Wilhelms [1990]
241 or Tanaka et al. [2014] definitions in favor of a more generic terminology. However, definitions
242 for "geomorphic unit" vary widely across the terrestrial and planetary literature and in the
243 context of terrestrial mapping, a geomorphic unit is most commonly used to refer to a landform
244 or group of landforms whose shape, structure, dimensions, or characteristics are indicative of a
245 common process (e.g., *Haskins et al.* [1998]).

246 In this study, the term "orbital facies" is used instead of "geologic unit" or "geomorphic
247 unit" since designations and subdivisions made from orbital visible-range images here were
248 based solely on variable brightness, local-scale color hue (spectral) variability, and surface
249 texture at a local and small scale. This term was first introduced by *Grotzinger and Milliken*
250 [2012] for that purpose. Orbital facies mapped using HiRISE images may indeed be geologic, or
251 geomorphic units according to the definitions employed by *Wilhelms* [1990], *Tanaka et al.*
252 [2014], or others and can be interpreted as such with supporting observations particularly from
253 topographic (i.e., interpretive geologic cross-sections) or rover-based datasets. However, the

254 reason for using the term "orbital facies" here (sensu *Grotzinger and Milliken* [2012]) is to
255 clarify that surface areas distinguished locally at the small scale employed during this study's
256 mapping can, but need not have three-dimensional geometry, substantial thickness, a common
257 formation process, a temporal association, nor must they represent lithified bedrock. Such an
258 objective approach also prevented the need to distinguish primary depositional from secondary
259 modification features from orbital images where such interpretations would have been uncertain
260 and speculative.

261 Orbital facies maps at the 1:500 scale were produced for each waypoint using a 240 m by
262 360 m rectangular area around the Darwin, Cooperstown, and Kimberley waypoints, respectively
263 using 25 cm/pixel HiRISE color and grayscale images (Figures 2 and 3). The intention of
264 mapping at this scale was to enable orbital facies distinctions of the highest level of detail
265 possible with orbital images for comparison with rover observations. Orbital facies contacts were
266 mapped as shapefiles on map-projected grayscale and color HiRISE mosaics in ArcGIS. To test
267 whether orbital facies represented stratigraphic units that could be reasonably projected into the
268 subsurface, interpretive cross-sections were constructed for each waypoint using topographic
269 profiles across the mapping area of each waypoint extracted from DTMs created by the HiRISE
270 team for the MSL project [*Kirk et al.*, 2008; *Golombek et al*., 2012; *Calef et al.*, 2013] (Figures
271 4, 7, 9). Although a number of subsurface interpretations are likely possible for each cross-
272 section, an attempt was made to present straightforward interpretations assuming approximately
273 horizontal strata and superposition (younger strata overlie older strata) since structural features
274 indicating otherwise were generally lacking in the study areas.

275 The grayscale visual and topographic basemaps providing coverage over the study areas
276 were made from twelve grayscale HiRISE 25 cm/pixel stereo pairs that were processed,

georeferenced, and projected via the methods of *Calef et al.* [2013] to create a visible mosaic and a DTM with 1 m grid spacing and absolute elevations tied to Mars Orbiter Laser Altimeter (MOLA) data. The processing of the HiRISE color mosaic used throughout this work (Figure 3) to aid in orbital geologic mapping interpretations was performed using a combination of the Integrated Software for Imaging Spectrometers (ISIS) (e.g., *Anderson et al.* [2004]; *Edmundson et al.* [2012]) and the davinci software packages (http://davinci.asu.edu). Data in this case were tied and projected to existing basemaps via a series of manually and automatically chosen ground control points used to update the spacecraft and camera pointing [*Edmundson et al.*, 2012]. Prior to map projection, the images were normalized for CCD-to-CCD variations within a single image. After map projection, the data were normalized for image-to-image variations to account for spatial and temporal variations such as illumination and observing geometry as well as atmospheric opacity. An across-track filter was used to remove any additional across-track image slope, and the normalized radiance data were stretched using a running (or moving-window) histogram stretch following the techniques described by *Edwards et al.* [2011]. This specialized stretch is designed to emphasize local-scale morphology and color variations by maximizing the dynamic range on a ~5000x5000 pixel segment of the image and also serves to remove any residual regional influence [*Edwards et al.*, 2011]. The resulting color HiRISE mosaic highlights the local-scale color (spectral) variability, where blue-purple hues commonly indicate mafic materials (e.g., sand dunes, blocks) and neutral colors (e.g., gray) indicate dustier terrains.

3.2 Rover Image-Based Mapping

Prior to arrival at each waypoint stop, the focusable Mastcam M-100 (100 mm fixed focal length) camera was used to acquire context mosaics. In this study, one mosaic was chosen for

each waypoint that provided a "rover's eye view" of as much of the orbital mapping area as possible (Figures 5, 8, and 10). Each of the waypoint mosaics was color corrected and perspective projected. Mosaics were used to map visible distinctions that fall into three general categories: bedrock outcrop lithology, surficial unconsolidated deposits, and undifferentiated bedrock outcrop and surficial deposits (Figure 6). Boundaries of bedrock outcrops define areas in which a particular lithology dominates and include conglomerates and sandstones of varying bedding characteristics. Although pixel scale varies within each mosaic and between mosaics, the mosaic pixel scale is generally on the order of ~1 cm/pixel or better for the majority of outcrop visible within each scene, permitting distinctions between outcrops of conglomerate and those containing sand-sized or finer grains as well as the identification of textural elements such as vugs and platy versus apparently massive beds. Where multiple lithologies occur together and subdivisions are difficult to define due to image resolution or interbedding, the outcrop is designated as "undifferentiated." Unconsolidated surficial deposits include sand, accumulations of float, defined here as loose pebble- to boulder-sized rocks not clearly connected to an outcrop, and undifferentiated sand and float. Where unconsolidated surficial deposits occur on outcrop exposures, and both are present and visible over a mappable area, undifferentiated surficial deposits and outcrop are mapped, e.g., "undifferentiated sandstone and float" or "undifferentiated conglomerate and float." As was the case for the orbital facies mapped from the HiRISE images, the outcrop lithologies and unconsolidated surficial deposits mapped in the rover mosaics can, but do not necessarily, represent distinct stratigraphic or geomorphic units.

To enable the comparison between orbital and rover-based observations, the distribution of orbital facies for each waypoint was mapped on the corresponding rover mosaics by identifying key landmark features in both the Mastcam mosaics and HiRISE images (Figures 5,

323 8, 10). Foreshortening and the different viewing geometry between orbital and ground-based
324 images complicates the translation of orbital facies mapped in plan-view onto the rover mosaics,
325 so the distribution of orbital facies mapped on rover mosaics should be considered approximate,
326 though generally faithful to the corresponding locations mapped on HiRISE images.
327 The stratigraphy for each waypoint was captured using the observations of lithology,
328 texture, and fabric gleaned from Mastcam M-100 mosaics and MAHLI images (Figures 6 and
329 11). To construct the stratigraphic columns, contact science outcrop locations were localized in
330 HiRISE orbital images relative to the rover traverse and distinctive features visible in both rover
331 mosaics and orbital images. Elevation values for the top and bottom of each outcrop were then
332 extracted from the HiRISE DTM and matched with geo-referenced rover stereo mosaics from the
333 Curiosity navigation cameras (Navcam) [*Maki et al.*, 2012] to calculate outcrop thickness.
334 Changes in bedding, grain-size, and erosional profile were then plotted in a stratigraphic column
335 for each contact science location (Figure 11). The rover-based stratigraphic column was then
336 plotted alongside the corresponding orbital facies projected as stratigraphic units for each contact
337 science location (Figure 11).
338 *Vasavada et al.* [2014] provided an overview of the outcrop characteristics observed at
339 both the Darwin and Cooperstown waypoints. This study expands on those results, presenting the
340 first annotated rover-based mosaics and stratigraphic columns for the express purpose of making
341 direct comparisons between rover and orbiter geologic interpretations.
342
343 **4. Orbiter and Rover Image-Based Mapping Observations**
344 **4.1. Darwin**
345 **4.1.1 Orbital Facies**

Five orbital facies were mapped at the Darwin waypoint: smooth dark, smooth hummocky, boulder hummocky, resistant cratered outcrop, and bright outcrop orbital facies (Figure 4). The resistant cratered outcrop orbital facies and the bright outcrop orbital facies are interpreted to represent lithified bedrock outcrop characterized by the presence of small scarps, visible stratification, and in a few locations the retention of craters. The bright outcrop orbital facies is characterized by its distinct brightness visible in the grayscale HiRISE image compared to the surrounding terrain (Figures 2b and 3). This orbital facies exhibits meter-scale variations in surface texture indicated by apparent changes brightness and/or shadows, m-scale polygonal fracture forms, and bright and dark alternations suggestive of bedding, although these textures are not ubiquitous throughout the entire exposure of this orbital facies. The bright outcrop orbital facies appears white and tan in the HiRISE color mosaic and exhibits color variation likely caused by the presence of float blocks or small-scale accumulations of windblown mafic sand on the outcrop. The bright outcrop orbital facies occurs primarily in the sub-circular plan-form feature at the center of the mapping area, although several occurrences of bright outcrop are mapped within the surrounding smooth hummocky orbital facies. The resistant cratered outcrop orbital facies is distinguished by the presence of impact craters that have diameters at decimeter-scale, a variable surface texture suggested by the meter-scale changes in relative brightness and color hue, and accumulations of dark boulders on the scarps that demarcate the boundaries of this unit. This orbital facies forms a scarp-forming capping material expressed at the tops of local topographic highs.

The smooth dark, boulder hummocky, and smooth hummocky orbital facies contain visible boulders and lack well-defined scarps, bedding, or craters. For these reasons, these three orbital facies are interpreted to represent unconsolidated surficial deposits. The smooth

hummocky orbital facies is mapped predominantly in the area surrounding the sub-circular bright outcrop in the center of the study area, and is characterized by a generally uniform brightness and decimeter-scale hummocky topography (Figure 2). In the HiRISE color image (Figure 3), this orbital facies appears tan to brown in color indicating that it may include a layer of surface dust. The boulder hummocky orbital facies appears similar in morphology to the smooth hummocky orbital facies, but contains accumulations of dark boulders resolvable in HiRISE images, and occurs in decimeter-scale areas within the bright outcrop orbital facies at the center of the Darwin mapped area. The smooth dark orbital facies is mapped and distinguished primarily with the aid of the HiRISE color mosaic as it is characterized by a distinctly blue hue consistent with the presence of mafic materials (e.g., basaltic sands). This facies occurs in topographic lows, and is interpreted as unconsolidated basaltic sand.

Two possible cross-sectional interpretations of the orbital facies observed at Darwin projected into the sub-surface as stratigraphic units are presented in Figure 4. In the first interpretation (Figure 4b), the bright outcrop orbital facies is interpreted as the infill of a bowl-shaped basin whose substrate material is composed primarily of the smooth hummocky facies. The bright outcrop orbital facies, which occurs both in the basin and outside the basin, might represent erosional remnants of a more continuous layer. In this scenario, the smooth hummocky orbital facies is the oldest of the five facies. The resistant cratered outcrop, boulder hummocky, and smooth dark orbital facies were deposited after the bright outcrop orbital facies. In the second interpretation (Figure 4c), the bright outcrop orbital facies is interpreted as a through-going horizontal layer in the subsurface rather than as a basin fill. In this model, the resistant cratered outcrop orbital facies directly overlies the bright outcrop orbital facies. The smooth hummocky, smooth dark, and boulder hummocky orbital facies are interpreted as discontinuous

accumulations of surficial deposits overlying both the bright outcrop and resistant cratered outcrop orbital facies.

4.1.2 Rover Image-Based Observations

The M-100 Mastcam mosaic of the Darwin waypoint shows a landscape dominated by exposures of conglomerate and sandstone bedrock overlain by localized sand drifts and fields of float (Figures 5 and 6a-c). Several conspicuous accumulations of dark, fine-grained float are observed in the mosaic, predominantly occurring on local topographic highs. Extending across the center of the mosaic is a topographic depression containing bedded and thin resistant-bedded sandstone outcrops and the occasional coarser-grained conglomerate bed exposed amongst undifferentiated accumulations of sand and float. Sandstone beds observed along the edges of the depression appear to dip toward the center of the basin such that dip varies systematically around the depression while outcrops near the middle of the basin show near horizontal dips. The bright exposure of sandstone and conglomerate present on the northwestern edge of the basin (right side, foreground of the Darwin mosaic) is the location of contact science activities performed by Curiosity and is documented in detail in the stratigraphic column in 11. A basal pebble conglomerate is overlain by a ~50 cm-thick layer of very coarse sandstone containing coarser-grained pebble-rich lenses. A discontinuous wedge of a cobble-bearing conglomerate overlies the sandstone interval and thin lenses of platy sandstone occur within this coarser-grained interval. These platy lenses occur in both horizontal and vertical orientations. A ~1.5 m-thick interval of massive granule conglomerate fines upward to coarse sandstone and overlies the cobble conglomerate. The section is capped by an accumulation of dark, fine-grained float.

4.1.3 Comparison between Orbiter and Rover Image-Based Mapping

As expected, a comparison of the mapped distributions of orbital facies and rover image-based bedrock lithologies and surficial deposits (Figure 5b and 5c) shows the increased level of detail and distinction possible with rover image observations. In addition, the rover-based observations permit the identification of specific bedrock lithologies (e.g., sandstone and conglomerate), rock type (i.e., sedimentary), and a confirmation of whether surface exposures represent lithified bedrock outcrop or unconsolidated surficial deposits. The smooth hummocky orbital facies, interpreted from orbit images as a likely unconsolidated deposit, is observed on the ground to be composed of in-place sandstone and conglomerate outcrop intermixed with float blocks. Although the presence of in-place rock outcrops was not resolvable in the HiRISE images of the smooth hummocky orbital facies, there is a fairly good correlation between this orbital facies and areas mapped as either float or undifferentiated sandstone and conglomerate. Similarly, the resistant cratered outcrop facies exhibits a fairly consistent correlation with accumulations of dark fine-grained float exposed at the top of local topographic highs. However, the rover mosaic shows that the resistant cratered outcrop orbital facies does not appear to correspond to actual lithified, in-place rock outcrop, but rather surficial concentrations of float blocks. There is a generally good correlation between the mapped distribution of the smooth dark orbital facies and areas containing higher proportions of surficial sand or undifferentiated sand and float. This correlation is particular apparent within the central depression at Darwin and is consistent with the orbital interpretation of the smooth dark orbital facies as a surficial deposit containing windblown sand. The bright outcrop orbital facies also corresponds fairly well with sandstone outcrops observed in Curiosity rover images, although the annotated rover mosaic shows the sandstone to be less extensive than the orbital mapping would indicate due to the presence of surficial sand and float (Figure 5c). The areas of bright outcrop orbital facies at the

contact science location correspond to an exposure of undifferentiated sandstone and conglomerate containing little surficial sand or float cover and which appears to be coarser grained than the sandstones cropping out in the central depression. The weakest correlation between an orbital facies and rover observations is seen with the boulder hummocky orbital facies, which fails to correspond directly to any unique outcrop lithology or surficial deposit observed in the rover mosaic. In the HiRISE image, the boulder hummocky orbital facies is distinguished primarily by the presence of resolvable boulders, but when these areas are observed on the ground in the Mastcam mosaic, the presence of in place sandstone and conglomerate outcrop becomes the primary characteristics by which these areas are distinguished.

4.2. Cooperstown

4.2.1 Orbital Facies

The smooth dark, boulder hummocky, smooth hummocky, resistant cratered outcrop, and bright outcrop orbital facies mapped at the Darwin area are also observed in HiRISE images of the Cooperstown waypoint. The bright outcrop orbital facies mapped at Cooperstown appears to be bluer in the HiRISE color image than that mapped at Darwin, perhaps indicating a greater proportion of mafic sand cover on the outcrop (Figure 3). Two orbital facies not present at Darwin were observed in the Cooperstown area: the bright striated outcrop and bright fractured outcrop orbital facies. The bright striated outcrop orbital facies occurs as a small isolated outcrop in the lower right part of the mapping area and is characterized by its relative brightness in the grayscale HiRISE mosaic and a white to tan color in the HiRISE color mosaic. Most distinctive however, are the northeast-southwest trending lineations that occur across the bright striated

outcrop orbital facies exposure at approximately even meter-scale spacing. At Cooperstown, the bright fractured outcrop orbital facies is distinguished from surrounding bright outcrop orbital facies by the presence of distinct meter-scale polygonal fractures and a bright white-yellow color in the HiRISE color mosaic.

The bright outcrop orbital facies mapped in the northeastern portion of the Cooperstown area forms a sub-circular outcrop shape in planform, possibly indicating a crater fill. However, other occurrences of the bright outcrop orbital facies are interpreted to extend in the subsurface throughout the mapping area as horizontal layers with the resistant cratered outcrop conformably overlying the bright outcrop facies strata (Figure 7b). The smooth hummocky, smooth dark, and boulder hummocky orbital facies are interpreted as unconsolidated surficial deposits overlying the resistant cratered and bright outcrop units, for the same reasons discussed for these orbital facies at the Darwin waypoint.

4.2.2 Rover Image-Based Observations

The Cooperstown M-100 mosaic shows an area dominated by sandstone outcrops of variable texture, grain size, and bedding characteristics (Figures 6d-f, 8a and 8c). The foreground of the Cooperstown mosaic includes an exposure of dark, fine-grained sandstone containing centimeter-scale vugs (Figure 6e). The dark, vuggy sandstone transitions into exposures of inter-bedded platy, cross-stratified and more thickly bedded (cm-scale beds) sandstone that occur on both the left and right sides of the mosaic (Figure 6d). This interval is overlain by sandstone with apparently massive texture. The massive sandstone is overlain by a distinct, erosion-resistant bed of pebbly sandstone. Several float accumulations occur in the Cooperstown area (Figure 6f), including a mound near the center of the mosaic separating the two inter-bedded platy and

bedded sandstone outcrops. Float and intermittent sandstone outcrops dominate the rest of the area imaged in the mosaic.

The stratigraphic section measured at the Cooperstown contact science location shows a basal interval of cross-stratified fine-grained sandstone overlain by nearly a meter massive coarse-grained sandstone that exhibits a sharp irregular basal contact (11). Granule-sized clasts are present within the coarse-sandstone, as are thin platy lenses similar to those observed at the Darwin outcrop. The massive coarse-grained sandstone is overlain by a pebbly sandstone containing fine-grained, highly angular, and irregularly shaped clasts.

4.2.3 Comparison between Orbital and Rover Image-Based Mapping

The comparison of orbital facies with bedrock and surficial deposits observed in the Cooperstown M-100 Mastcam mosaic is illustrated in Figure 8. The smooth dark orbital facies corresponds to some, but not all, of the areas mapped as float in the rover mosaic. Other occurrences of float in the area were mapped in the orbital images as resistant cratered outcrop, smooth hummocky, and bright outcrop orbital facies (Figures 8b and 8c). The boulder hummocky orbital facies corresponds well with an accumulation of dark float of a fine-grained lithology observed in the rover mosaic as expected since the largest of the boulders are visible in HiRISE (Figures 2 and 3). The resistant cratered outcrop orbital facies appears to correspond most directly with outcrops exposed on local topographic highs but does not correspond uniquely to a particularly lithology or type of surficial deposit. For example, the outcrop of vuggy sandstone visible in the foreground of the Cooperstown rover mosaic corresponds to an area mapped as resistant cratered outcrop orbital facies, as is the resistant pebble sandstone bed and a mound of float located in the center of the mosaic field of view (Figures 8b and 8c). While the resistant cratered outcrop orbital facies corresponds to a variety of bedrock lithologies observed

505 on the ground, the mapped boundaries of this orbital facies do correspond consistently with
506 contacts between sandstone lithologies that show variable resistance to erosion. As at Darwin,
507 the bright outcrop orbital facies at Cooperstown is well correlated with outcrops of apparently
508 massive, bedded, and platy sandstone viewed by the rover.

509 **4.3. Kimberley**

510 **4.3.1 Orbital Facies**

511 Three additional orbital facies were mapped at the Kimberley waypoint (smooth
512 hummocky outcrop, smooth boulder outcrop, and bright bedded outcrop orbital facies) in
513 addition to orbital facies discussed previously (Figure 9). As at Darwin and Cooperstown, the
514 smooth hummocky orbital facies observed at Kimberley rarely forms scarps, appears smooth on
515 a meter-scale, and exhibits no sign of internal stratification. Therefore it is interpreted as an
516 unconsolidated surficial deposit. However, there are small patches exposed within the smooth
517 hummocky orbital facies that exhibit variable surface texture, appear to shed small boulders, and
518 in some occurrences retain craters. These areas are more similar in brightness and color hue to
519 the smooth hummocky orbital facies rather than the bright outcrop orbital facies and do not
520 exhibit scarps as is common around exposures of the resistant cratered outcrop orbital facies.
521 Therefore, these areas are mapped as a new orbital facies, the smooth hummocky outcrop. The
522 smooth boulder outcrop orbital facies is distinguished by the presence of rounded hills that are
523 uniform in tone and color and appear generally smooth except for the accumulations of boulders
524 found on the sides of the hills. The bright bedded outcrop orbital facies appears gray and tan in
525 the HiRISE color mosaic and is characterized by horizontal bedding planes visible in the orbital
526 images. This orbital facies lacks the textural diversity apparent in the bright striated and bright
527 fracture outcrop orbital facies. Although a small exposure of the bright striated orbital facies was

528 observed in the Cooperstown area, this orbital facies is more extensively present in the
529 Kimberley area. From examining the HiRISE images alone, it is difficult to ascertain the origin
530 of the striations that distinguish this orbital facies. But at Kimberley, the striations are observed
531 to be so linear within individual outcrop exposures that several possibilities exist to explain the
532 geometry of these features: (1) the striations are defined by surface lineations rather than planes
533 that extend into the subsurface, (2) the striations are defined by planes (e.g. beds) having an
534 inclination that is steep relative to changes in outcrop topography, or (3) the striations are defined
535 by three dimensional curved planes, but outcrop topography consistently counteracts the
536 curvature of these planes. The first two options are likely the most plausible, albeit
537 indistinguishable from HiRISE images alone, while the third option requires a more contrived set
538 of circumstances and is therefore less likely.
539 The well-exposed and clearly defined outcrops visible in HiRISE at the Kimberley
540 waypoint enable an interpretation of the bright striated outcrop, bright bedded outcrop, and
541 smooth hummocky orbital facies as stratigraphic rock units that can be projected into the
542 subsurface with greater confidence than at the previous waypoints. The cross-section presented
543 in Figure 9b illustrates the interpreted relative age relationship between these orbital facies; the
544 stratigraphically lowest and hence oldest facies exposed in this area is the bright striated outcrop
545 orbital facies, which is overlain by the bright bedded outcrop and smooth hummocky orbital
546 facies. The topographic profile extracted across the bright striated outcrop orbital facies shows 1-
547 2 meters of variable topography on the contact between this orbital facies and the overlying
548 bright bedded orbital facies. Buttes of the smooth boulder outcrop and the resistant cratered
549 orbital facies are interpreted to overlie the bright bedded outcrop facies, although the relative age
550 relationship between the smooth boulder and the resistant cratered orbital facies is unknown. The

551 smooth hummocky, boulder hummocky, and smooth dark orbital facies are best interpreted as
552 unconsolidated surficial deposits that overlie eroded outcrops of the bright bedded, striated, and
553 fractured outcrop orbital facies, as well as the resistant cratered and smooth boulder outcrop
554 orbital facies. The smooth hummocky outcrop orbital facies may be an exception to this
555 relationship.

556 **4.3.2 Rover Image-Based Observations**

557 The Kimberley M-100 mosaic covers an outcrop of south-dipping coarse-grained
558 sandstone beds with variable resistance to erosion (Figures 6g and Figure 10). Coarse sandstone
559 beds containing granule-sized clasts underlie the south-dipping beds. Fine-grained sandstones
560 showing no preferential southward dip overlie the south-dipping sandstone beds (Figure 6h). The
561 three hills visible at the Kimberley outcrop are primarily covered in float (Figure 6i), although
562 each hillside exhibits apparently massive sandstone interstratified beds. The terrain surrounding
563 the Kimberley outcrop is largely covered in unconsolidated accumulations of float.

564 The stratigraphic column shown in Figure 11 was constructed from observations made at
565 the location of the Windjana drill site at the southeastern edge of the Kimberley outcrop. Here,
566 coarse granule sandstone underlies the sandstone beds that transition from primarily horizontal to
567 south-dipping orientations. The south-dipping strata are overlain by cross-stratified very fine-
568 grained sandstone beds bounded at the base by a sharp, undulatory contact. The cross-stratified
569 sandstone is overlain by sandstones of a grain size that is not resolvable in the Mastcam images
570 and was not observed with MAHLI, but appears to be relatively fine-grained. Coarse-grained,
571 possiblly south-dipping beds are observed within this interval, but the presence of float and cover
572 make it difficult to identify sedimentary structures or bedding within this interval. An
573 accumulation of dark float occurs at the top of the hill (informally named Mount Remarkable).

574 **4.3.3. Comparison between Orbiter and Rover Image-Based Mapping**

575 The comparison of orbiter versus rover image-based observations shown in Figure 10
576 reveals a relatively good correlation between orbital facies contacts and contacts observed in the
577 Kimberley Mastcam mosaic between distinct lithologies and surficial deposits. Due to the well-
578 exposed outcrop at the Kimberley waypoint, there is a nearly perfect correlation between the
579 mapped distribution of bright striated outcrop orbital facies and the south-dipping resistant and
580 recessive sandstones mapped in the rover mosaic (Figures 10b and 10c). Using rover image-
581 based observations of the bright striated outcrop orbital facies, the three possibilities for the
582 origin of the striations observed in HIRISE images described in the previous section can be re-
583 evaluated. The presence of south-dipping sandstone beds of variable resistance in areas mapped
584 as bright striated outcrop orbital facies indicate that the striations cannot be completely explained
585 as surface lineations (option 1), but are due in large part to the intersection of inclined bedding
586 planes with the modern day erosional outcrop topography (option 2). There is no evidence from
587 ground-based rover observations that the bedding planes are curved, so option 3 can be
588 eliminated.

589 Areas mapped as float in the rover mosaic correspond to the smooth hummocky orbital
590 facies, and areas containing a higher proportion of sand to float are generally mapped in the
591 HIRISE images as smooth dark orbital facies. The bright bedded outcrop orbital facies
592 corresponds well with flat-lying platy sandstone beds mapped in the Mastcam mosaic, and the
593 contact between these platy sandstones and underlying south-dipping sandstone beds is identified
594 with high fidelity in both the orbital map and rover mosaic. The three hills present at the
595 Kimberley waypoint were mapped in HiRISE images as smooth boulder outcrop orbital facies
596 which corresponds to accumulations of fine-grained float and intermittent exposures of

sandstone on the slopes of the hills. The smooth appearance of these hills in orbital images is likely due to accumulations of sand and float on the hilltops.

5. Discussion

The comparison between mapped orbital facies and rover-image based distinctions of bedrock lithologies and unconsolidated surficial deposits at the Darwin, Cooperstown, and Kimberley waypoints illustrates several important points about the utility and validity of orbital geologic map interpretations. Orbital facies mapping is useful for distinguishing lithified in-place outcrop from unconsolidated deposits, and can be used to identify geologically significant contacts if outcrop exposure is good and adjacent facies exhibit differences in brightness, surface texture, or weathering characteristics such as resistance to erosion. This is particularly important since datasets such as THEMIS-derived thermal inertia (100 m/pixel) and CRISM (~18 m/pixel), which can also provide information about physical and compositional differences on the surface, have resolutions too coarse to allow meaningful distinction between orbital facies mapped at the scale employed in this study. At all three waypoints, the bright outcrop orbital facies, including the bright striated, bright bedded, and bright fractured outcrop orbital facies, were correctly identified during HiRISE mapping as in-place, lithified rock outcrops. The resistant cratered outcrop facies was also correctly identified as lithified rock at Cooperstown and Kimberley. The smooth dark, boulder hummocky, and smooth hummocky orbital facies were correctly identified from orbital images as largely unconsolidated surficial deposits, although the exception is the smooth hummocky orbital facies mapped at Darwin, where intermittent exposures of sandstone and conglomerate bedrock could not be resolved from orbital images. The ability to distinguish between lithified rock outcrop and unconsolidated surficial deposits is important and particularly

620 useful for planning rover science investigations and traverse and mobility assessment. In-place
621 rock outcrops rather than unconsolidated deposits, are often the desired science target for
622 stratigraphic and geologic investigations of depositional processes, paleoenvironment, and
623 geochemistry of ancient sedimentary rocks. Conversely, terrain consisting of unconsolidated
624 surficial deposits may be favored over in place outcrop when planning traverses that minimize
625 wheel damage and hazard to the roving vehicle [*Yingst et al.*, 2014].

626 Orbital facies maps can also be useful for recognizing distinct contacts between bedrock
627 units, particularly when accompanied by a clear topographic scarp or mappable differences in
628 brightness, color, or surface texture. The ability to recognize significant geologic contacts from
629 orbiter image datasets is particularly important for making strategic decisions during mission
630 surface operations that determine where a rover is sent to address hypotheses about the geologic
631 nature of the site. Orbital geologic interpretations initially guided the MSL team in its decision to
632 drive the Curiosity rover to Yellowknife Bay [*Grotzinger et al.*, 2014; *Palucis et al.*, 2014], and
633 several examples from this study illustrate the utility of orbital facies mapping for identifying
634 geologically significant contacts. At the Cooperstown waypoint, the mapped contact between the
635 resistant cratered outcrop and the bright outcrop orbital facies in the vicinity of the contact
636 science location represents a sharp transition between the massive and platy-bedded fine
637 sandstone beds and the resistant pebbly sandstone. At Kimberley, where the outcrops are well-
638 exposed and orbital facies are easily distinguished in HiRISE images, the orbital map
639 interpretations provided sufficient information to identify the contact between south-dipping
640 coarse sandstone beds and the overlying flat-lying platy sandstones, a stratigraphic relationship
641 that was critical for determining the origin of the enigmatic striations observed in HiRISE
642 images.

643 There are also ways in which orbital map interpretations are limited, particularly when
644 used alone without corresponding datasets acquired on the ground. Differences in relative
645 brightness, color, or textural characteristics observed in orbital image datasets may indeed be
646 suggestive of inherent differences in the material properties of bedrock units, but these orbital
647 characteristics can be non-unique and heavily biased by unconsolidated materials exposed
648 immediately at the surface. For example, the presence and distribution of thin, discontinuous
649 surficial deposits of float, sand, and dust may result in the distinction of multiple orbital facies
650 within the same geological unit due to changes in color and brightness caused only by these
651 mantling materials. The two alternate cross-section interpretations presented for the Darwin
652 waypoint illustrate this point. In the first cross-section (Figure 4b), the smooth hummocky orbital
653 facies observed at the surface is interpreted as a distinct and important stratigraphic unit of at
654 least several meters thickness that forms the substrate of the basin in which younger facies were
655 deposited. In contrast, in the second cross-section interpretation (Figure 4c) the smooth
656 hummocky orbital facies is interpreted as a relatively thin mantle deposit that is obscuring more
657 extensive underlying exposures of bright outcrop and resistant cratered outcrop orbital facies.
658 The two interpretations have very different implications for the timing and relative age
659 relationship of the outcrops and deposits observed from orbital datasets and on the ground as
660 well as the timing of basin formation, yet it is challenging to distinguish between the two
661 hypotheses using the orbital image data. This is not surprising, and in fact supports the rationale
662 for sending rovers to the surface of planetary bodies as it is difficult to ascertain the degree of
663 heterogeneity at outcrop scale from orbit, and to interpret the significance of that heterogeneity.
664 As another example of the non-uniqueness of orbital facies interpretations, consider two
665 areas (Darwin vs. Cooperstown) that exhibit similar remote sensing properties. At the Darwin

666 waypoint, the resistant cratered outcrop orbital facies corresponds to accumulations of
667 unconsolidated float blocks. In contrast, the resistant cratered outcrop orbital facies at
668 Cooperstown corresponds to a variety of in-place, lithified sandstone outcrops. Some of the
669 outcrops mapped as resistant cratered orbital facies at Cooperstown were fine-grained and
670 vuggy, whereas others were coarse-grained and contained pebble-size clasts, likely representing
671 very different depositional conditions and/or processes. Based solely on the orbital mapping,
672 these resistant cratered outcrop facies occurrences could be interpreted and correlated as co-eval
673 deposits of a similar origin, but rover-based observations show that such a correlation would not
674 be valid. In addition, the bright outcrop orbital facies mapped at all three Curiosity waypoints
675 may suggest that a time-rock correlation of these orbital facies could be appropriate. However, a
676 closer examination of the bedrock outcrop with rover images at each waypoint (Figure 11), calls
677 into question the validity of such a correlation. At Darwin, the bright outcrop orbital facies
678 corresponds to an outcrop of coarse sandstones and pebble conglomerates whereas the bright
679 outcrop mapped at Cooperstown corresponds to fine-grained platy-bedded and massive
680 sandstones. While a general regional correlation between these two locations may still be
681 possible, the rover data reveal no clear rationale for a geologic correlation of the contact between
682 the bright outcrop and overlying resistant cratered outcrop orbital facies mapped at Darwin with
683 that same orbital facies contact mapped at Cooperstown.
684 The orbital and in situ comparisons presented in this study also illustrate the difficulty in
685 making process-based interpretations from orbital mapping alone, particularly in areas like
686 Bradbury Rise in Gale crater where present-day topography and geomorphology provide few
687 indications of past depositional process or paleoenvironment. For comparison, there are some
688 locations on the surface of Mars where depositional interpretations are possible based almost

689 solely on orbital observations, as is the case for inverted relief features such as channels or
690 preserved fans or deltas, volcanic constructs such as lava flow lobes, or impact ejecta deposits.
691 The Peace Vallis fan in Gale crater is an example of such a deposit. The present-day topography
692 of this feature enables its identification as an alluvial fan, for which calculations of total volume
693 and runoff can be made [*Palucis et al.*, 2014]. The distribution of inverted channel features and
694 measurements of present-day fan slope also allows an evaluation of the relative importance of
695 various depositional processes contributing to fan formation, particularly the role of distributary
696 channel formation versus sheet flow, debris flow, and mud flow deposition throughout the fan
697 [*Palucis et al.*, 2014]. Furthermore, the location of Yellowknife Bay at the distal end of the Peace
698 Vallis fan led the MSL team to hypothesize that fine-grained sediments representing deposition
699 in a lacustrine setting might be found there, a hypothesis that was "field checked" and proven
700 correct by observations from the Curiosity rover [*Grotzinger et al.*, 2014; *Palucis et al.*, 2014].
701 In contrast, Bradbury Rise lacks diagnostic paleogeomophic features such as those characterizing
702 the Peace Vallis fan and unlike Yellowknife Bay, Bradbury Rise shows no clear temporal or
703 spatial relationship with the Peace Vallis fan. Therefore, distinguishing a process-based
704 sedimentary origin for the three waypoints examined in this study from orbital image data alone
705 is admittedly challenging. In these cases, rover image-based observations of lithology, grain
706 size, and texture are essential for interpreting depositional hypotheses.
707 As a consequence of the various limitations described above, it is common practice for
708 orbital stratigraphic interpretations to show simple "layer cake" stratigraphic models in which
709 orbital facies are interpreted as stratal units of relatively constant thickness, horizontal
710 deposition, and lateral continuity at least at the scale of the drafted cross-section. This is usually
711 the simplest model to interpet the data. The cross-sections presented for each waypoints in

712 Figures 4, 7, and 9 are modeled by this "layer cake" geometry, as is the regional schematic cross-
713 section of Bradbury Rise incorporating all three waypoints shown in Figure 12a. Because the
714 geometry of subsurface units in these examples provides no indication of a process-based
715 depositional interpretation of the stratigraphic units, more complex stratigraphic models, though
716 plausible, would likely be an over-interpretation of the available data and thus speculative.
717 Although some "layer cake" models may be valid representations of the subsurface geology, in
718 situ observations of the bedrock outcrop and surficial deposits present at the three waypoints in
719 Gale crater suggest that a more appropriate model for the subsurface of Aeolis Palus is that
720 shown in the schematic in Figure 12b. In this model, the fundamental principles of stratigraphy
721 still hold, but lithologic units exposed at the surface are mapped and interpreted in the context of
722 the fluvial depositional system suggested for Bradbury Rise by the in situ analysis of *Williams et*
723 *al.* [2013], *Grotzinger et al.* [2014], and *Vasavada et al.* [2014]. Such a model for the subsurface
724 stratigraphy is likely closer to reality for fluvial depositional systems than the layer cake model
725 presented in Figure 12a, but its construction was only suggested with in situ rover interpretations
726 of the outcrop lithologies exposed throughout Aeolis Palus.
727
728 **6. Implications for mapping future landing sites on Mars**
729 High-resolution orbital images have been incredibly important for increasing recent
730 understanding of the geological diversity of the martian surface and have made a positive impact
731 on surface mission landing site selection and surface operations, but this study shows that even
732 25 cm/pixel HiRISE images mapped at a 1:500 scale will provide limited to no information
733 about the small-scale textural characteristics of an outcrop, including grain size, lithology, or
734 internal structures (e.g., bedforms and fine-scale bedding characteristics), that are critical for

735 making depositional interpretations even as fundamental as sedimentary versus volcanic. The
736 vertical viewing geometry of orbital imaging systems can also limit the amount of geologically
737 significant information gleaned from outcrop exposures observed in orbital data, particularly
738 because three dimensional outcrop exposures are difficult to observe in orbital data. Yet orbital
739 images provide a breadth of surface coverage and the local-to-regional context for detailed rover
740 observations that the limited visual range and horizontal viewing geometry of a ground-based
741 rover cannot provide, highlighting how complementary the combined approach of orbiter and
742 rover-image based analysis can be.

743 Developing more complex and detailed process-based models for the depositional history
744 of martian landing sites through the integration of small-scale detailed orbital geologic mapping
745 and analysis of rover image datasets is critical for making better informed predictions of where
746 ground-based rovers missions like Curiosity or future rovers might concentrate effort and
747 resources to find preserved evidence of past habitable environments, organic matter, or other
748 biosignatures. Ground-based rovers are needed to measure small-scale textural characteristics of
749 rock outcrops, such as grain size, lithology, sedimentary structures, bedding style, and allow the
750 exploration of three-dimensional outcrop exposures that are essential for paleoenvironmental
751 reconstructions. Small-scale orbital mapping of high-resolution image datasets like that carried
752 out in this study aids in the planning and execution or rover measurements on daily or monthly
753 operational timescales and provides critical context for these measurements at a finer-scale than
754 that typically employed in regional or global orbital geologic map investigations.

755 As critical as the integration of orbiter and rover data is for understanding the past
756 depositional processes and paleoenvironments on the surface of Mars, the reality is that rover
757 and landed missions to Mars are rare and the majority of the planet can only be studied with

orbital data sets. Although it may not be practical to map large areas of the martian surface at the 1:500 scale (or finer) employed for the waypoint study areas here, for locations on Mars considered of interest for future rover or even human missions, the analysis of high resolution orbital image datasets through fine-scale orbital geologic mapping efforts are important for mission planning purposes as well as predicting in advance the diversity of rock outcrops and deposits that will be encountered.

This study highlighted some of the considerable challenges that persist with geologic interpretations of the highest resolution orbital images currently available of the martian surface, but future airborne or orbital imaging systems designed to image at even higher resolutions could help resolve the limitations of existing orbital geologic interpretations. Imaging at the ~1-5 cm/pixel scale would afford the ability to recognize finer distinctions in outcrop texture that could significantly aid in the depositional interpretation of orbital facies and the recognition of locally and regionally significant geologic contacts.

7. Conclusions

The Curiosity rover stopped at three locations, the Darwin, Cooperstown, and Kimberley waypoints during its traverse from Yellowknife Bay to the base of Aeolis Palus. This study presents detailed orbital geologic maps for each waypoint based on HiRISE grayscale and color images, and provides a comparison between orbital facies and bedrock outcrop and surficial deposits observed at each waypoint with images from the Curiosity rover Mastcam M-100 and MAHLI cameras. The results of the orbiter and rover-based comparison are as follows:

(1) Orbital facies mapping is generally useful for distinguishing between lithified in-place bedrock outcrop and unconsolidated surficial deposits.

(2) Orbital facies mapping can be used to identify distinct contact boundaries if outcrop exposure is good and adjacent facies exhibit differences in brightness, color hue, surface texture, or resistance to erosion.

(3) The remote sensing properties used to identify and define orbital facies from orbital images, and the interpretations that results from observations of these properties, can be non-unique and biased by a mapper's interpretation of how distinct those properties are, leading to challenges in accurately correlating spatially distinct orbital facies.

(4) Process-based interpretations based on orbital image observations alone should be made cautiously for landscapes such as Bradbury Rise which lack clear paleogeomorphic landforms or topography indicative of a particular depositional process.

(5) Stratigraphic architecture interpreted from orbital maps is often represented as "layer cake" models, but these models are inconsistent with Curiosity rover observations of the ancient sedimentary environments explored in Gale crater. Integration of orbiter and rover image-based observations is needed to construct more sophisticated stratigraphic or depositional models.

(6) Fine-scale orbital mapping of future candidate landing sites, actual landing sites, and field investigation traverse paths like that presented in this study, integrated with rover image-based observations enables better informed predictions of where ground-based missions like Curiosity or future rovers might concentrate effort and resources to find preserved evidence of past habitable environments, organic matter, or other biosignatures.

Acknowledgments

Funding to K. Stack Morgan for this work was provided by a Jet Propulsion Strategic Initiative Research and Technology Development grant. The authors would like to acknowledge the scientists and engineers of the MSL and MRO HiRISE missions, without whom the data and analysis presented in this paper would not have been possible.

References

Anderson, R. B. and J. F. Bell III (2010), Geologic mapping and characterization of Gale Crater and implications for its potential as a Mars Science Laboratory landing site, *Mars, 5*, 76-128, doi:10.1555/mars.2010.0004.

Anderson, J., S. Sides, D. Soltesz, T. Sucharski, and K. Becker (2004), Modernization of the integrated software for imagers and spectrometers, *Lunar and Planetary Science Conference*, *35*, 2039.

Arvidson, R. E. et al. (2006), Nature and origin of the hematite-bearing plains of Terra Meridiani based on analyses of orbital and Mars Exploration rover data sets, *J. Geophys. Res., 111*, E12S08, doi:10.1029/2006JE002728.

Arvidson, R. E., et al. (2008), Mars Exploration Program 2007 Phoenix landing site selection and characteristics, *J. Geophys. Res.,113*(E00A03), doi:10.1029/2007JE003021.

Arvidson, R. E., et al. (2014), Terrain physical properties derived from orbital data and the first 360 sols of Mars Science Laboratory Curiosity rover observations in Gale Crater, *JGR-Planets, 119*, 1322-1344, doi:10.1002/2013JE004605.

Arvidson, R. E. et al. (2015). Mars Reconnaissance Orbiter and Opportunity observations of Burns Formation and underlying strata: Crater-hopping at Meridiani Planum, *J. Geophys. Res. - Planets, 120*, doi:10.1002/2014JE004686.

Binder, A.B., Arvidson, R.E., Guinness, E.A., Jones, K.L., Morris, E.C., Mutch, T.A., Pieri, D.C. and Sagan, C. (1977). The geology of the Viking lander 1 site. *Journal of Geophysical Research, 82,* doi: 10.1029/JB082i028p04439.

Cabrol, N. A., E. A. Grin, H. E. Newsom, R. Landheim, C. P. McKay (1999), Hydrogeologic Evolution of Gale Crater and Its Relevance to the Exobiological Exploration of Mars, *Icarus, 139*, 235-245.

Calef, F. J., III, W. E. Dietrich, L. Edgar, J. Farmer, A. Fraeman, J. Grotzinger, M. C. Palucis, T. Parker, M. Rice, S. Rowland, K. M. Stack, D. Sumner, J. Williams, and the MSL Science Team (2013), Geologic Mapping of the Mars Science Laboratory Landing Ellipse, *Lunar and Planetary Science Conference, 44,* 2511.

Crumpler, L. S., R. A. Craddock, and J. C. Aubele (2001), Geologic map of the MTM 25047 and 20047 quadrangles, central Chryse Planitia/Viking 1 Lander site, Mars, IMAP 2693, U. S. Department of the Interior, U.S. Geological Survey.

Crumpler, L. S., et al. (2011), Field reconnaissance geologic mapping of the Columbia Hills, Mars, based on Mars Exploration Spirit and MRO HiRISE observations, *JGR-Planets, 116*(E00F24)*,* doi:10.1029/2010JE003749.

Crumpler, L. S. et al. (2015), Context of ancient aqueous environments on Mars from in situ geologic mapping at Endeavor Crater, *J. Geophys. Res., 120*(3), doi:10.1002/2014JE004699.

Edmundson, K. L., D. A. Cook, O. H. Thomas, B. A. Archinal, and R. L. Kirk (2012), JIGSAW: The ISIS3 Bundle Adjustment for Extraterrestrial Photogrammetry, *ISPRS Ann. Photogramm. Remote Sens. Spatial Inf. Sci.*, *I-4*, 203-208, doi:10.5194/isprsannals-I-4-203-2012.

Edwards, C. S., K. J. Nowicki, P. R. Christensen, J. Hill, N. Gorelick, and K. Murray (2011), Mosaicking of global planetary image datasets: 1. Techniques and data processing for Thermal Emission Imaging System (THEMIS) multi-spectral data, *J. Geophys. Res.*, *116*(E10), E10008, doi: doi:10.1029/2010JE003755.

Fergason, R. L., P. R. Christensen, M. P. Golombek, T. J. Parker (2012), Surface Properties of the Mars Science Laboratory Candidate Landing Sites: Characterization from Orbit and Predictions, *Space Sci Rev, 170,* 739-773, doi:10.1007/s11214-012-9891-3.

Golombek, M. P. et al. (2003), Selection of the Mars Exploration Rover landing sites, *JGR, 108*(E12), 8072, doi:10.1029/2003JE002074.

Golombek M. P. et al. (2005), Assessment of Mars Exploration Rover landing site predictions, *Nature, 436*, 44-48, doi:10.1038/nature03600.

Golombek, M. P. et al. (2006), Geology of the Gusev cratered plains from the Spirit rover transverse, *J. Geophys. Res., 11*(E02S07), doi:10.1029/2005JE002503.

Golombek, M. P. et al. (2008), Size-frequency distributions of rocks on the northern plains of Mars with special reference to Phoenix landing surfaces, *J. Geophys. Res., 113*(E00A09), doi:10.1029/2007JE003065.

Golombek, M. P. et al. (2012), Selection of the Mars Science Laboratory Landing Site, *Space Sci Rev, 170*, 641-737, doi:10.1007/s11214-012-9916-y.

Greeley, R. and J. E. Guest (1987), Geologic map of the eastern equatorial region of Mars: U.S. Geological Survey Miscellaneous Investigations Series Map I-1802-B, scale 1:15,000,000, U.S. Department of the Interior, U.S. Geological Survey.

Grotzinger, J. P. and R. E. Milliken (2012), The sedimentary rock record of Mars: Distribution, origins, and global stratigraphy, in *Sedimentary Geology of Mars,* SEPM Special Publication No. 102, edited by J. P. Grotzinger and R. E. Milliken, pp. 1-48, SEPM, Tulsa, O.K.

Grotzinger, J. P. et al. (2012), Mars Science Laboratory Mission and Science Investigation, *Space Sci. Rev., 170*, 5-55, doi:10.1007/s11214-012-9892-2.

Grotzinger J. P., et al. (2014), A Habitable Fluvio-Lacustrine Environment at Yellowknife Bay, Gale Crater, Mars, *Science, 343*, 1242777.

Hansen, V. L. (2000), Geologic mapping of tectonic planets, *Earth and Planet. Sci. Lett., 176*, 527-542.

Haskins et al. (1998), A Geomorphic Classification System, Version 1.4, Washington D.C., U.S. Department of Agriculture Forest Service, 110 p.

Jacob, S. R., S. Rowland, F. J. Calef III, K. M. Stack, and the MSL Team (2014), Characteristics and origin of a cratered unit near the MSL Bradbury landing site (Gale Crater, Mars) based on analyses of surface data and orbital imagery, *Lunar and Planetary Science Conference, 45*, 1395.

Jakosky, B.M. and Christensen, P.R. (1986). Global duricrust on Mars: Analysis of remote sensing data. *Journal of Geophysical Research 91,* doi: 10.1029/JB091iB03p03547.

LeDeit, L., E. Hauber, F. Fueten, M. Pondrelli, A. Pio Rossi, and R. Jaumann, Sequence of infilling events in Gale Crater, Mars: Results from morphology, stratigraphy, and mineralogy, *JGR-Planets, 118*, 2439-2473, doi:10.1002/2012JE004322.

Kirk, R. L., et al. (2008), Ultrahigh resolution topographic mapping of Mars with MRO HiRISE stereo images: Meter-scale slopes of candidate Phoenix landing sites, *J. Geophys. Res., 113*(E3), E00A24, doi:10.1029/2007JE003000.

Komatsu, G. and V. R. Baker (1997). Paleohydrology and flood geomorphology of Ares Vallis. *Journal of Geophysical Research, 102.* doi: 10.1029/96JE02564.

Maki, J. et al (2012). The Mars Science Laboratory Engineering Cameras, *Space Sci. Rev., 170,* 77-93, doi:10.1007/s11214-012-9882-4.

Milliken, R. E., J. P. Grotzinger, and B. J. Thomson (2010), Paleoclimate of Mars as captured by the stratigraphic record in Gale Crater, *Geophys. Res. Lett., 37*(L04201), doi:10.1029/2009GL041870.

Okubo, C. H. (2014). Bedrock geologic and structural map through the western Candor Colles region of Mars: U.S. Geological Survey Scientific Investigations Map 3309, pamphlet 8 p., scale 1:18,000, doi:10.3133/sim3309.

Palucis, M. C. et al (2014). The origin and evolution of the Peace Vallis fan system that drains to the Curiosity landing area, Gale Crater, Mars, *J. Geophys. Res.- Planets, 119,* 705-728, doi:10.1002/2013JE004583.

Rice, J. W. and Edgett, K. S. (1997). Catastrophic flood sediments in Chryse Basin, Mars, and Quincy Basin, Washington: Application of sandar facies model. *Journal of Geophysical Research 10,:* doi: 10.1029/96JE02824.

Rice, M. S., J. F. Bell III, S. Gupta, N. H. Warner, K. Goddard, and R. B. Anderson (2013a), A detailed geologic characterization of Eberswalde crater, Mars, *Mars, 8*, 15-57, doi:10.1555/mars.2013.0002.

Rice, M. S., J. M. Williams, F. Calef, R. B. Anderson, L. Edgar, K. Stack, D. Y. Sumner, H. E. Newsom, J. P. Grotzinger, P. King (2013b), Detailed geologic mapping along the Mars Science Laboratory (MSL) Curiosity traverse path from Glenelg to Mount Sharp, *Lunar and Planetary Science Conference*, *44*, 2892.

Scott, D. H. and M. H. Carr (1978), Geologic map of Mars: U.S. Geological Survey Mscellaneous Investigations Series Map I-1083, scale 1:25,000,000, U.S. Department of the Interior, U.S. Geological Survey.

Scott, D. H. and K. L. Tanaka (1986), Geologic map of the western equatorial region of Mars: U.S. Geological Survey Miscellaneous Investigations Series Map I-1802-A, scale 1:15,000,000, U.S. Department of the Interior, U.S. Geological Survey.

Seelos, K. D. et al. (2008), Geomorphologic and mineralogic characterization of the northern plains of Mars at the Phoenix Mission candidate landing sites, *J. Geophys. Res., 113*(E00A3), doi:10.1029/2008JE003088.

Smith, P. H. et al. (1997), Results from the Mars Pathfinder Camera, *Science, 278*(5344), 1758-1765, doi:10.1126/science.278.5344.1758.

Sumner, D. S. et al. (2013). Preliminary Geological Map of the Peace Vallis Fan Integrated with In Situ Mosaics From the Curiosity Rover, Gale Crater, Mars, *Lunar and Planetary Science Conference, 44,* 1699.

Sun, V. Z. and R. E. Milliken (2014). The geology and mineralogy of Ritchey crater, Mars: Evidence for post-Noachian clay formation, *J. Geophys. Res. Planets, 119,* 810-836, doi:10.1002/2013JE004602.

935 Tanaka, K. L. and D. H. Scott (1987), Geologic map of the polar regions of Mars, Geologic
936 Investigations Series Map I-1802-C, scale 1:15,000,000, U.S. Department of the Interior,
937 U.S. Geological Survey.
938 Tanaka, K. L., J. A. Skinner, Jr., L. S. Crumpler, and J. M. Dohm (2009). Assessment of
939 planetary geologic mapping techniques for Mars using terrestrial analogues: The SP
940 Mountain area of the San Francisco Volcanic Field, Arizona, *Planetary and Space*
941 *Science, 57*, 510-532, doi:10.1016/j.pss.2008.06.012.
942 Tanaka, K. L., J. A. Skinner, Jr., J. M. Dohm, R. P. Irwin, III, E. J. Kolb, C. M. Fortezzo, T.
943 Platz, G. G. Michael, and T. M. Hare (2014), Geologic Map of Mars, Scientific
944 Investigations Map 3292, U.S. Department of the Interior, U.S. Geological Survey.
945 Thomson, B. J. and P. H. Schultz (2007), The geology of the Viking Lander 2 site revisited,
946 *Icarus, 191*, 505-523, doi:10.1016/j.icarus.2007.05.011.
947 Thomson, B. J., N. T. Bridges, R. E. Milliken, A. Baldridge, S. J. Hook, J. K. Crowley, G. M.
948 Marion, C. R. de Souza Filho, A. J. Brown, C. M. Weitz (2011), Constraints on the origin
949 and evolution of the layered mound in Gale Crater, Mars using Mars Reconnaissance
950 Orbiter Data, *Icarus*(214), 413-432, doi:10.1016/j.icarus.2011.05.002.
951 Vasavada, A. R., J. P. Grotzinger, R. E. Arvidson, F. J. Calef, J. A. Crisp, S. Gupta, J. Hurowitz,
952 N. Mangold, S. Maurice, M. E. Schmidt, R. C. Wiens, R. M. E. Williams, and R. A.
953 Yingst (2014), Overview of the Mars Science Laboratory mission: Bradbury Landing to
954 Yellowknife Bay and beyond, *JGR-Planets, 119*, 1134-1161,
955 doi:10.1002/2014JE004622.
956 Wilhelms, D. E. (1990), Geologic mapping, in *Planetary Mapping*, edited by R. G. Greeley and
957 R. M. Batson, Cambridge Planetary Science Series 6, pp. 208-260, Cambridge University
958 Press, Cambridge.
959 Williams, R. M. E., et al. (2013), Martian Fluvial Conglomerates at Gale Crater, *Science,*
960 *340*(6136), 1068-1072, doi:10.1126/science.1237317.
961 Wiseman, S. M., et al. (2010), Spectral and stratigraphic mapping of hydrated sulfate and
962 phyllosilicate-bearing deposits in northern Sinus Meridiani, Mars, *Journal of*
963 *Geophysical Research: Planets*, *115*(E7), E00D18, doi:10.1029/2009JE003354.
964 Wray, J. J., E. Z. Noe Dobrea, R. E. Arvidson, S. M. Wiseman, S. W. Squyres, A. S. McEwen, J.
965 F. Mustard, and S. L. Murchie (2009), Phyllosilicates and sulfates at Endeavor Crater,
966 Meridiani Planum, Mars, *Geophys. Res. Lett., 36*(L21201), doi:10.1029/2009GL040734.
967 Yingst, R. A. et al. (2014). Terrain Assessment in Gale Crater from Sol 0-500 Using Orbital
968 Thermal Inertia and In Situ Visible Data, *Geological Society of America Annual Meeting*,
969 Vancouver, B. C., Paper No. 202-8.

970 **Tables**

971 **Table 1. Curiosity rover waypoints during the Bradbury Rise traverse**

Waypoint	Arrival Sol	Departure Sol	Curiosity Rover Geology Investigation
Darwin	392	401	Remote sensing (Mastcam and Chemcam) and Contact Science (APXS and MAHLI)
Cooperstown	441	443	Remote sensing (Mastcam and Chemcam) and Contact Science (APXS and MAHLI)
Kimberley	574	631	Remote sensing (Mastcam and Chemcam), Contact Science (APXS and MAHLI), Dust Removal Tool (DRT), Drill, CheMin, SAM

Figures

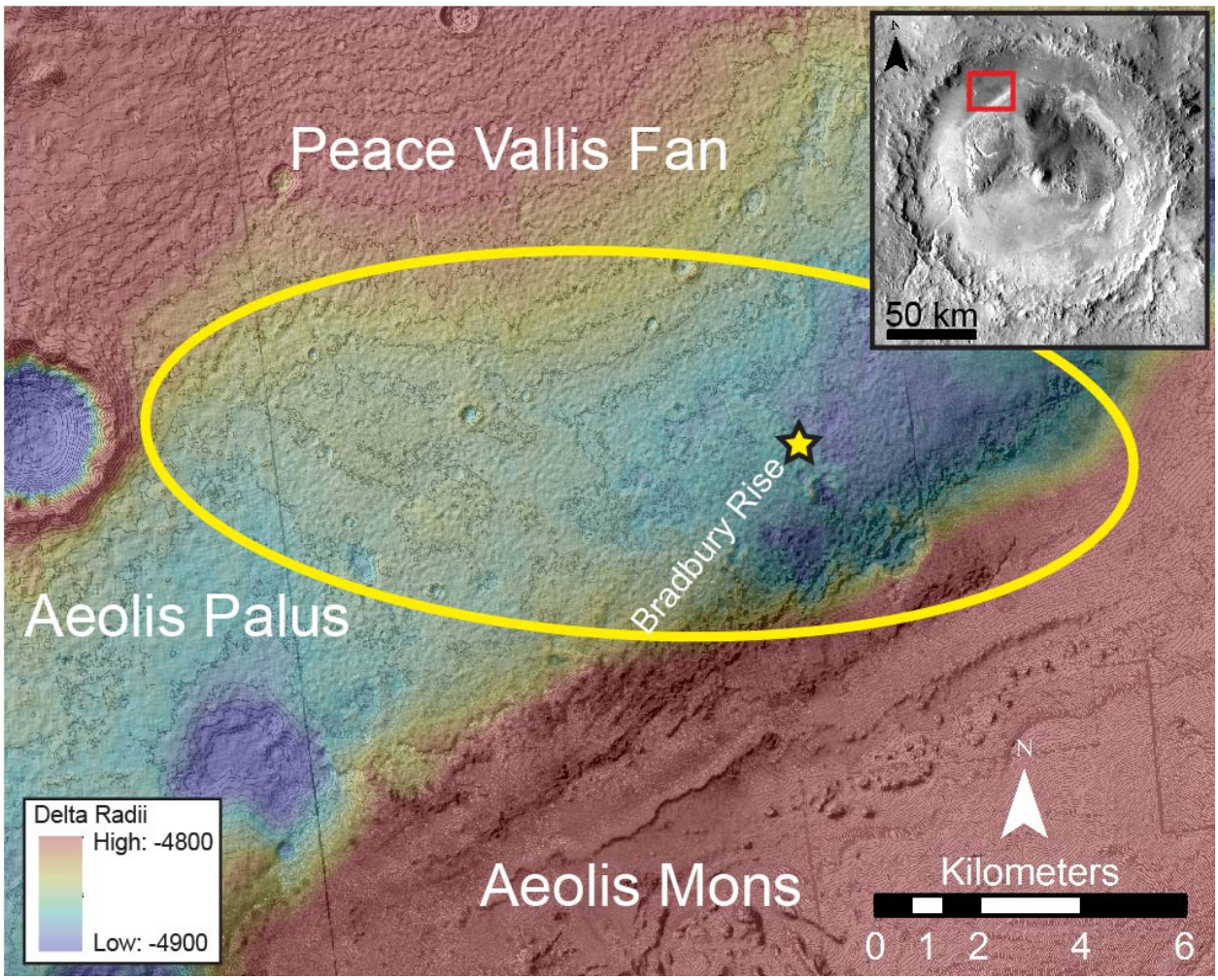

Figure 1. Mars Science Laboratory Curiosity landing ellipse (yellow ellipse), Curiosity landing site (yellow star), and location of Bradbury Rise annotated on a shaded relief topographic map of the Peace Vallis Fan, Aeolis Palus, and Aeolis Mons. Contours represent 10 m intervals. Inset figure shows Gale crater in THEMIS Day IR..

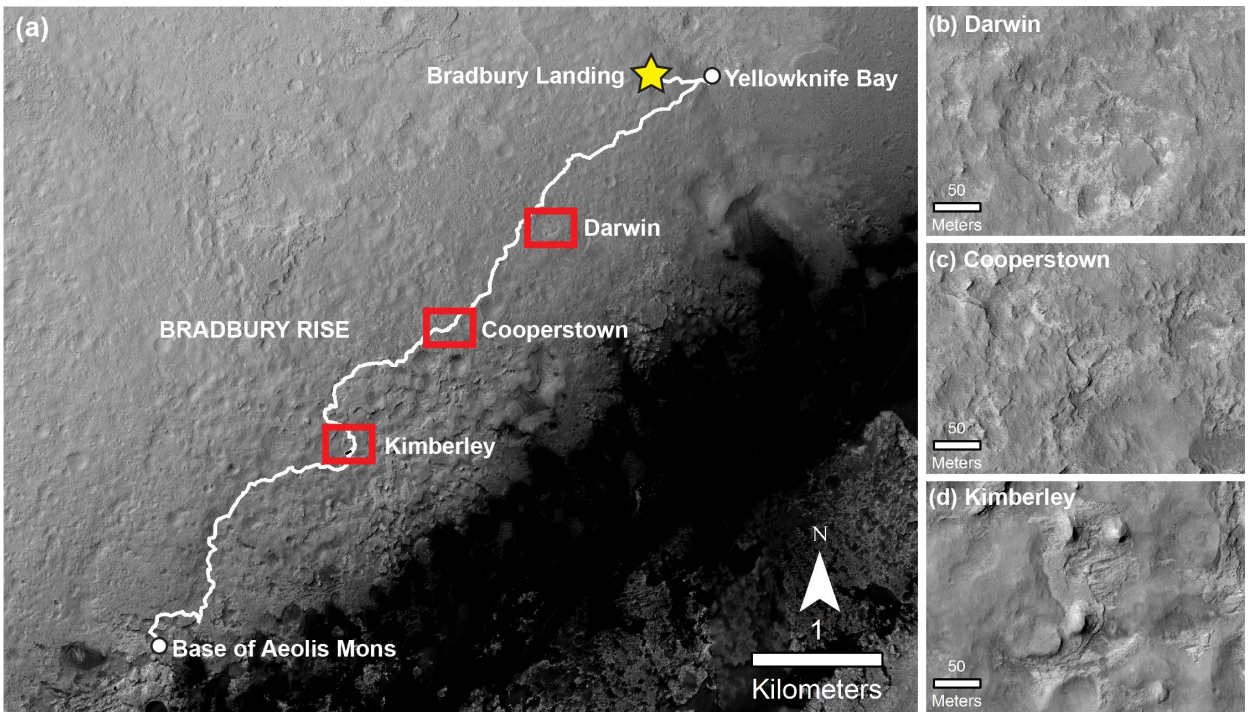

979

980 **Figure 2.** (a) HiRISE mosaic showing the Curiosity rover traverse across Bradbury Rise and the
981 locations of the Darwin, Cooperstown, and Kimberley waypoints in relation to Bradbury
982 Landing (yellow star), Yellowknife Bay, and the base of Aeolis Mons. (b) HiRISE image of the
983 Darwin, (c) Cooperstown, (d) Kimberley waypoints.

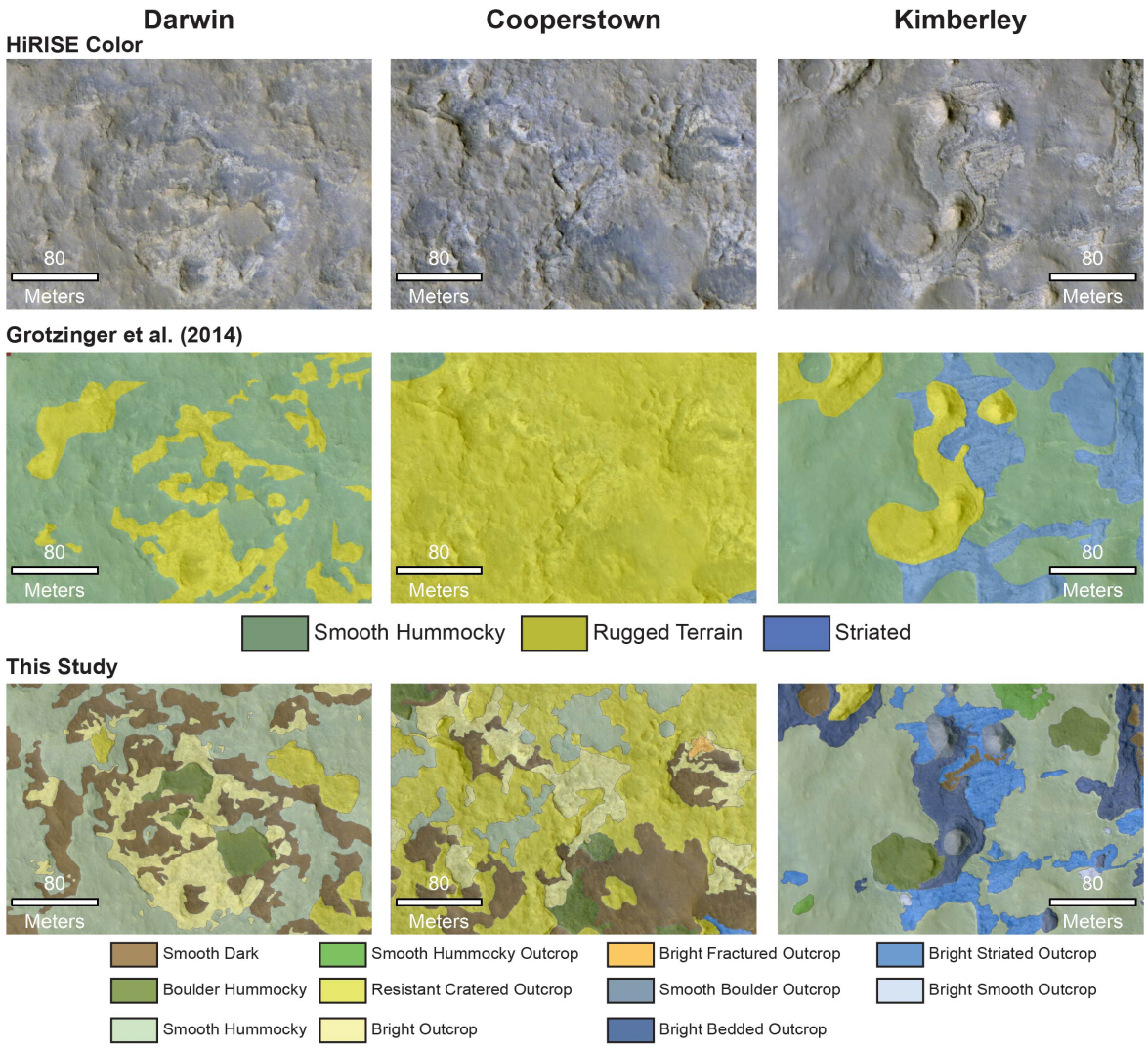

984

985 **Figure 3.** Previous orbital mapping effort of the Darwin, Cooperstown, and Kimberley waypoints by *Grotzinger et al.* [2014]

986 compared to this study's orbital maps.

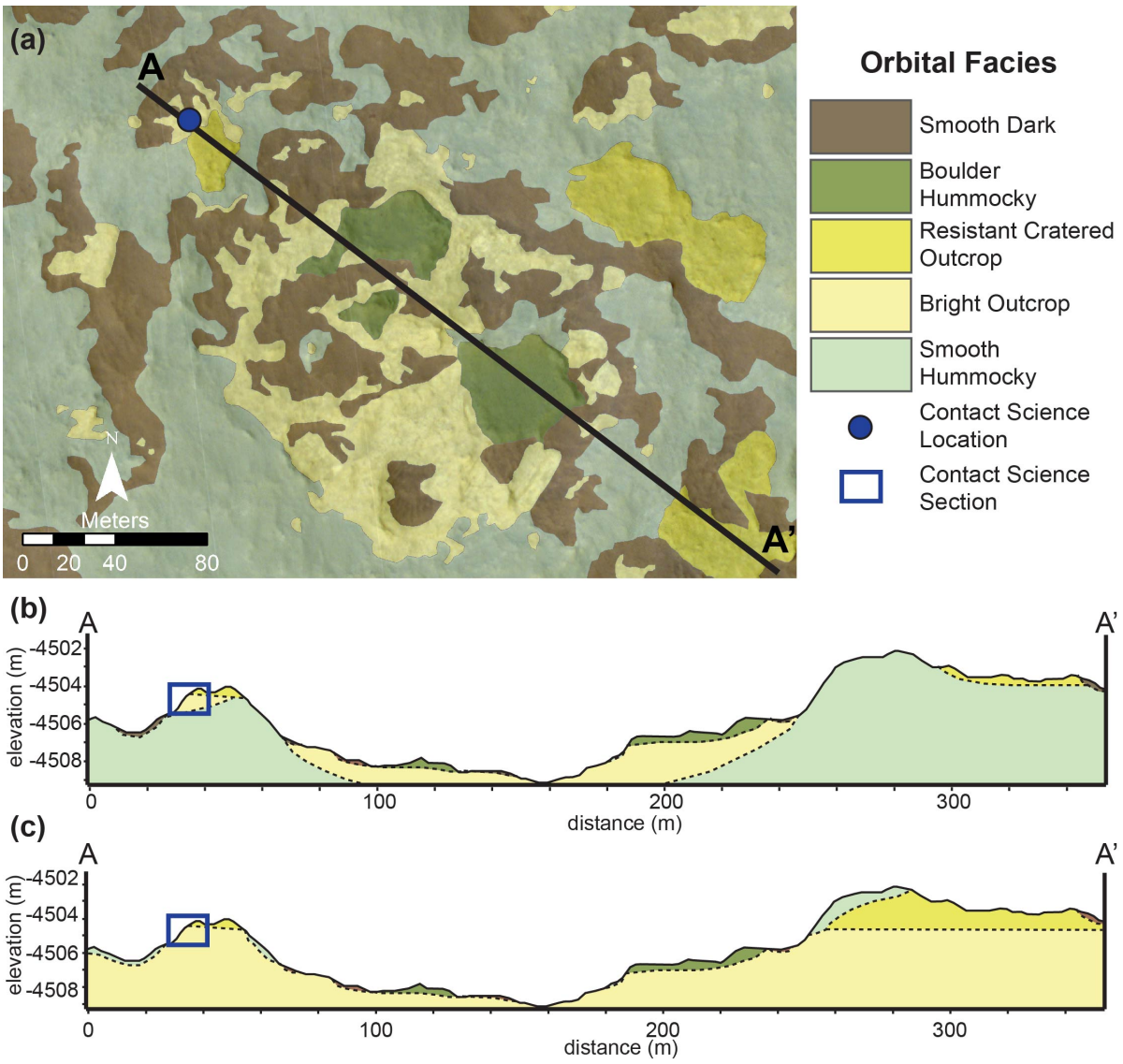

Figure 4. (a) Orbital facies map of the Darwin waypoint and (b-c) two alternate cross section interpretations representing A to A'. The rover's location when the mosaic in Figure 6 was acquired is just north of the mapping area displayed here. The Darwin contact science location used to construct the stratigraphic column in Figure 10 is indicated by the blue dot, and the section examined is outlined in the blue box in (b) and (c).

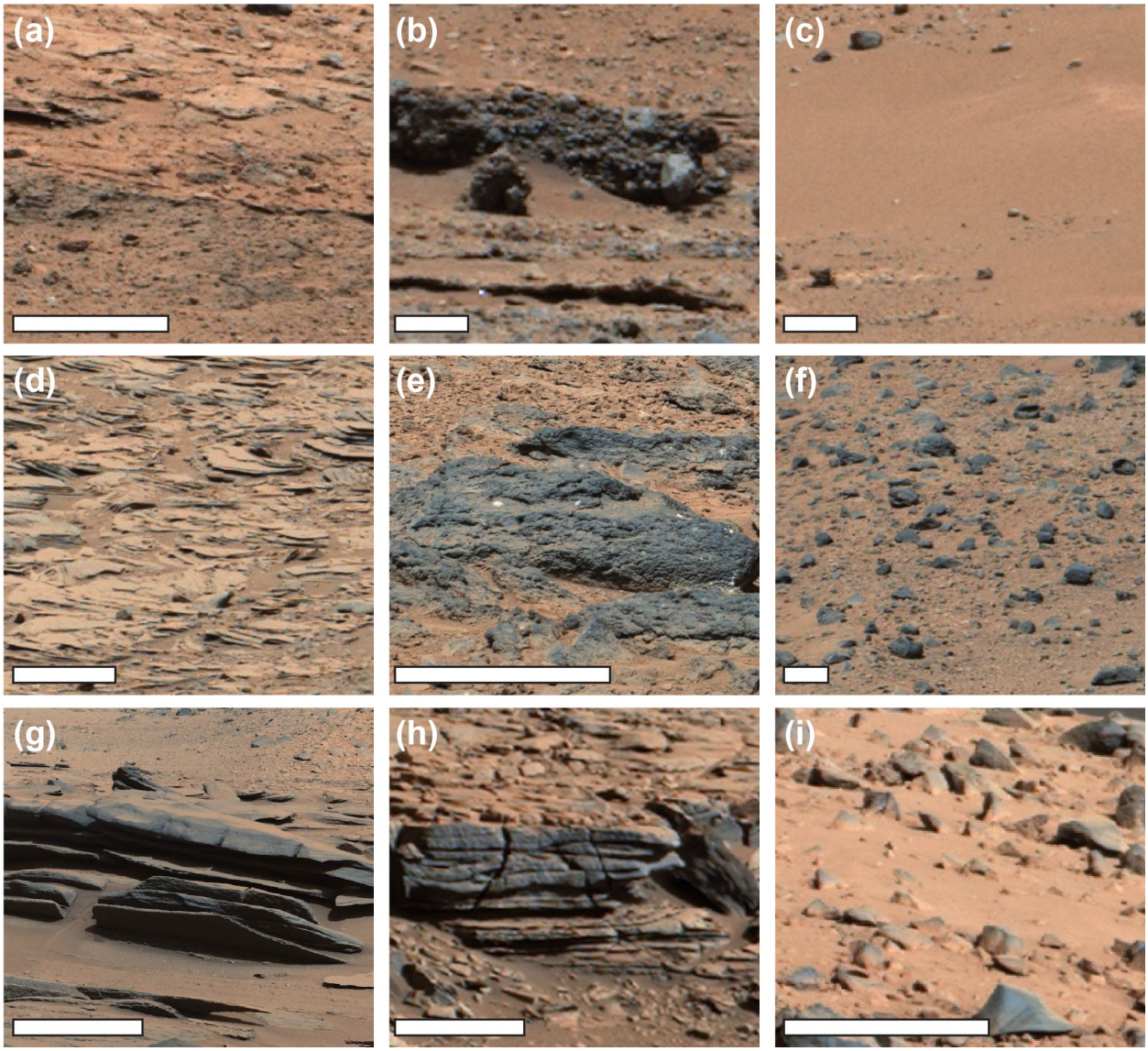

Figure 5. Representative examples of bedrock lithologies and surficial deposits observed in the M-100 rover mosaics of the Darwin (a-c), Cooperstown (d-f), and Kimberley (g-i) waypoints. Scale bar = 50 cm. Darwin: (a) undifferentiated sandstone and conglomerate, (b) conglomerate, (c) sand; Cooperstown: (d) platy sandstone, (e) vuggy sandstone, (f) dark float consisting of fine-grained boulders and cobbles; Kimberley: (a) south-dipping resistant and recessive sandstones, (b) bedded sandstone, (c) undifferentiated sand and float.

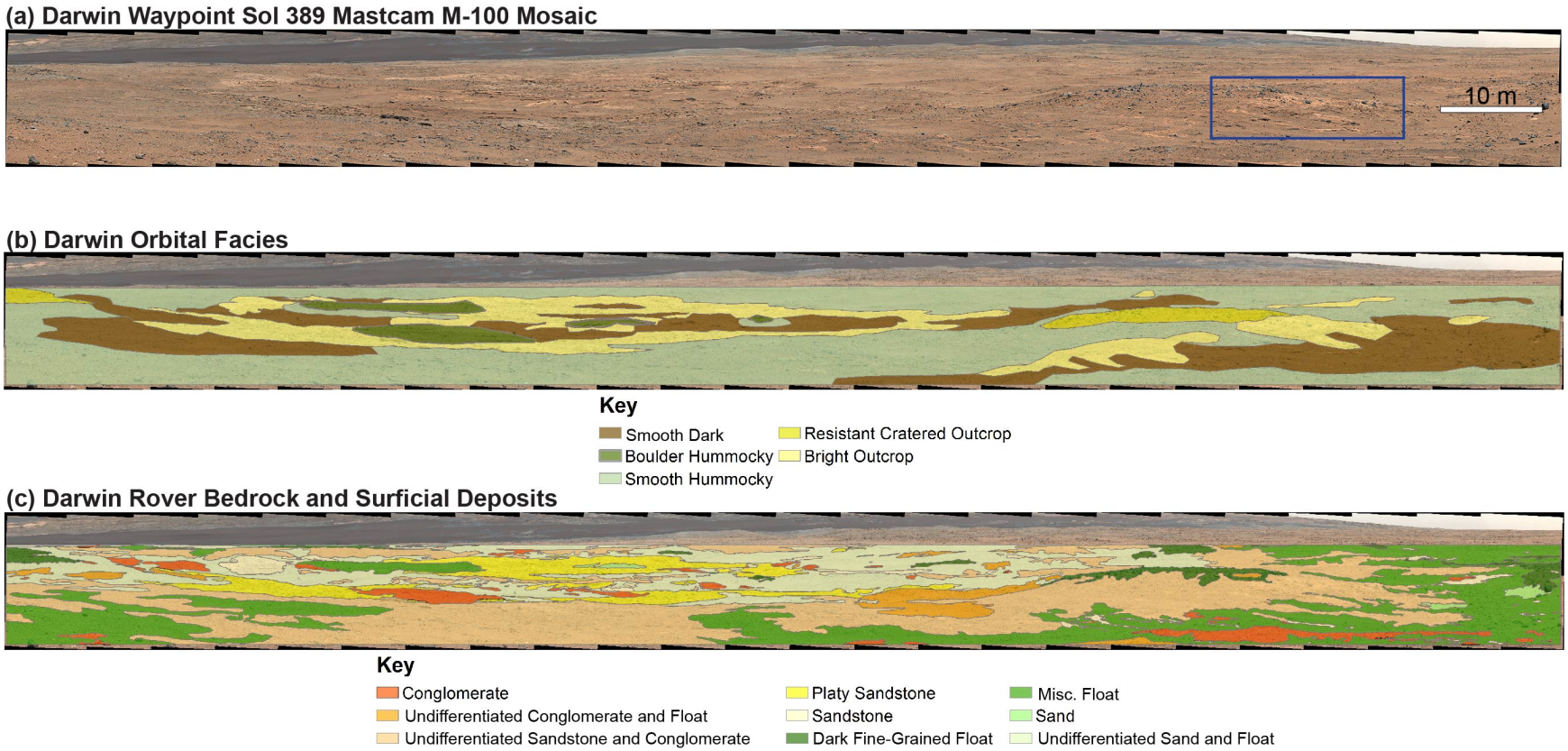

Figure 6. Rover mosaic of the Darwin waypoint. (a) Sol 389 Mastcam M-100 Mosaic. Blue box shows the portion of the Darwin outcrop examined with Curiosity's contact science instruments and represented in Figure 11a, (b) mosaic annotated with mapped orbital facies, (c) mosaic annotated with bedrock lithology and surficial deposit type observed in rover images.

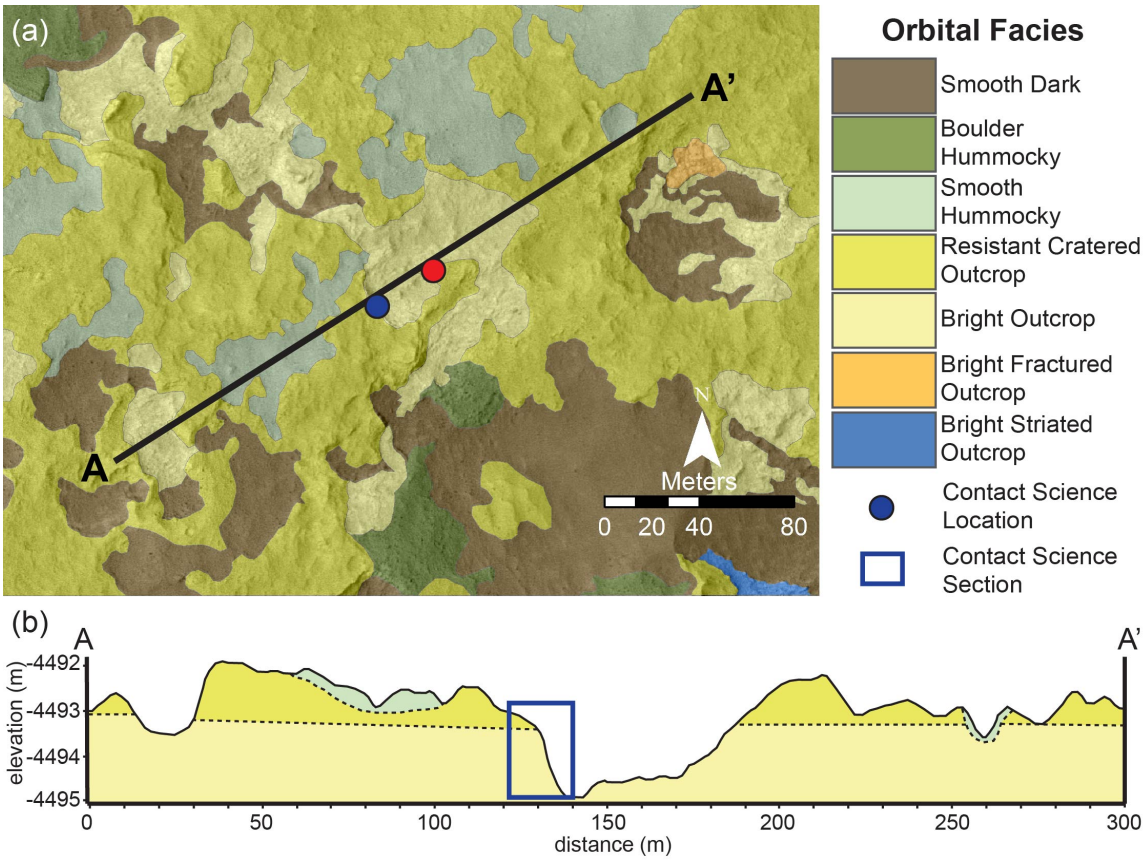

Figure 7. (a) Orbital facies map of the Cooperstown waypoint and (b) cross section interpretation representing A to A'. Red dot indicates the rover's location when the mosaic in Figure 8 was acquired. The Cooperstown contact science location used to construct the stratigraphic column in Figure 11 is indicated by the blue dot, and the section examined is outlined in the blue box.

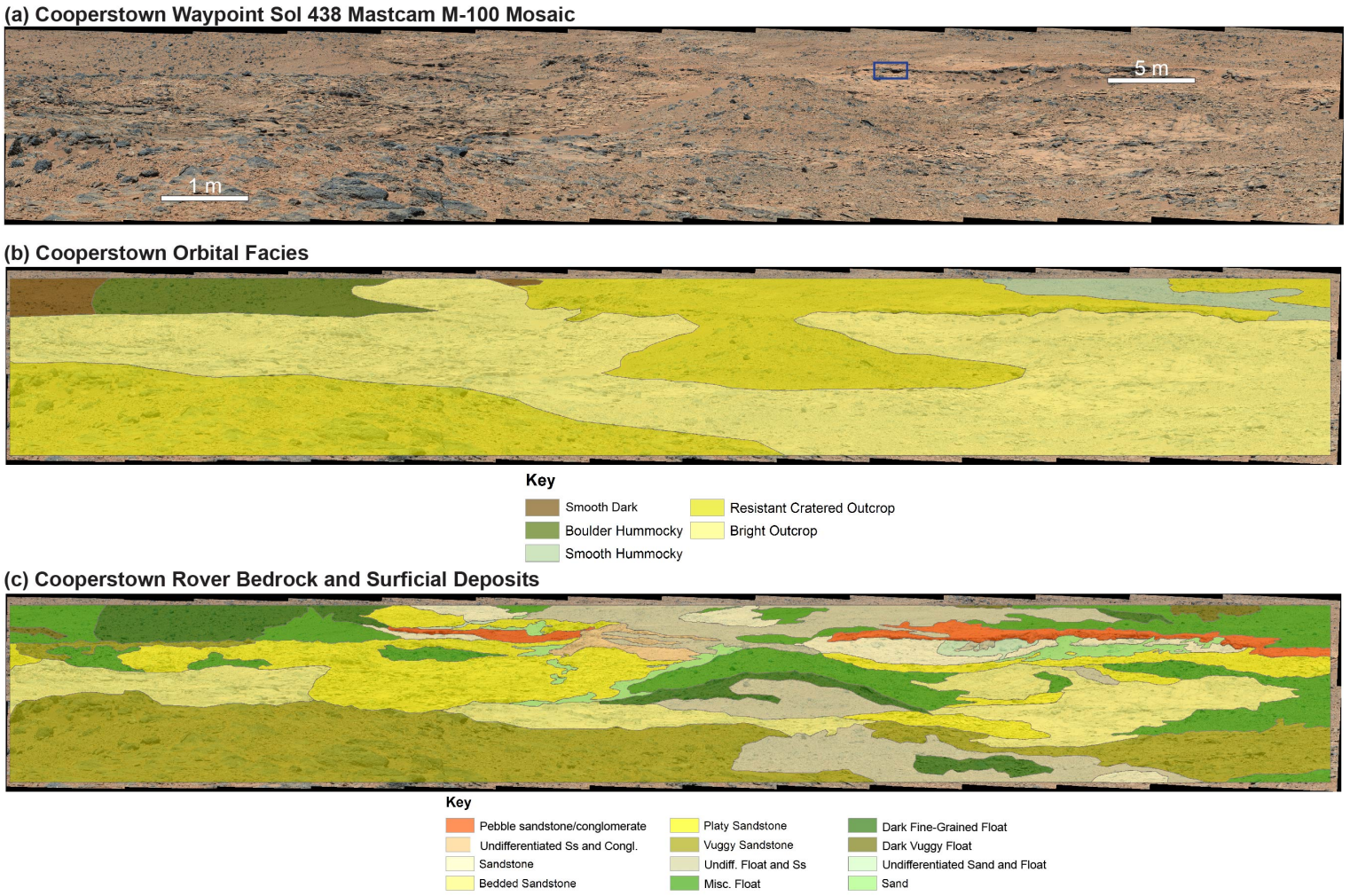

Figure 8. Rover mosaic of the Cooperstown waypoint. (a) Sol 438 Mastcam M-100 Mosaic. Blue box shows the portion of the Cooperstown outcrop examined with Curiosity's contact science instruments represented by the section in Figure 11b, (b) mosaic annotated with mapped orbital facies, (c) mosaic annotated with bedrock lithology and surficial deposit type observed in rover images.

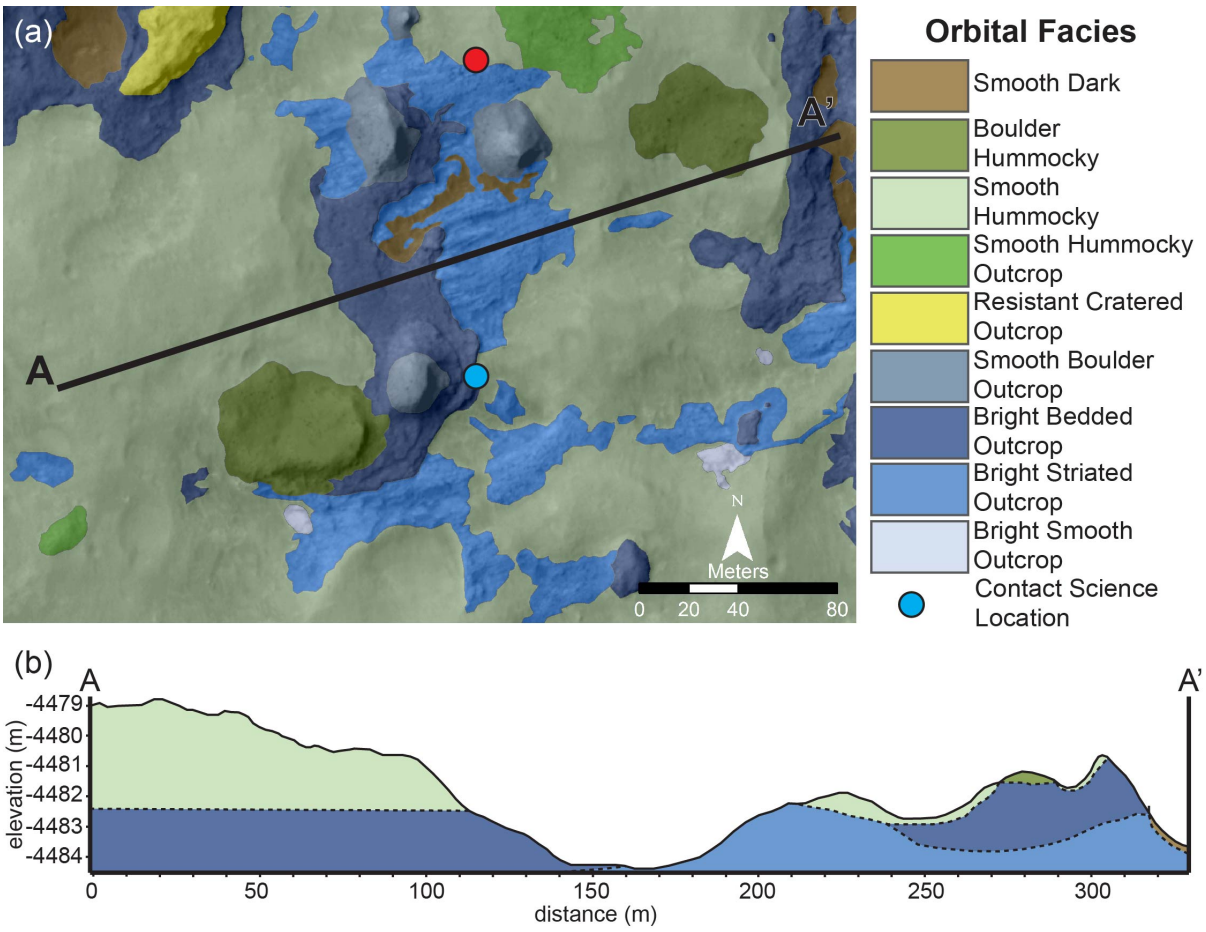

1017

1018 **Figure 9.** (a) Orbital facies map of the Kimberley waypointand (b) cross section interpretation

1019 representing A to A'. The red dot indicates the rover's location when the mosaic in Figure 10

1020 was acquired. The blue dot indicates the Windjana contact science and drill location used to

1021 construct the stratigraphic section in Figure 11c. Since the cross-section does not cross this

1022 location, no annotation of the section is shown in (b).

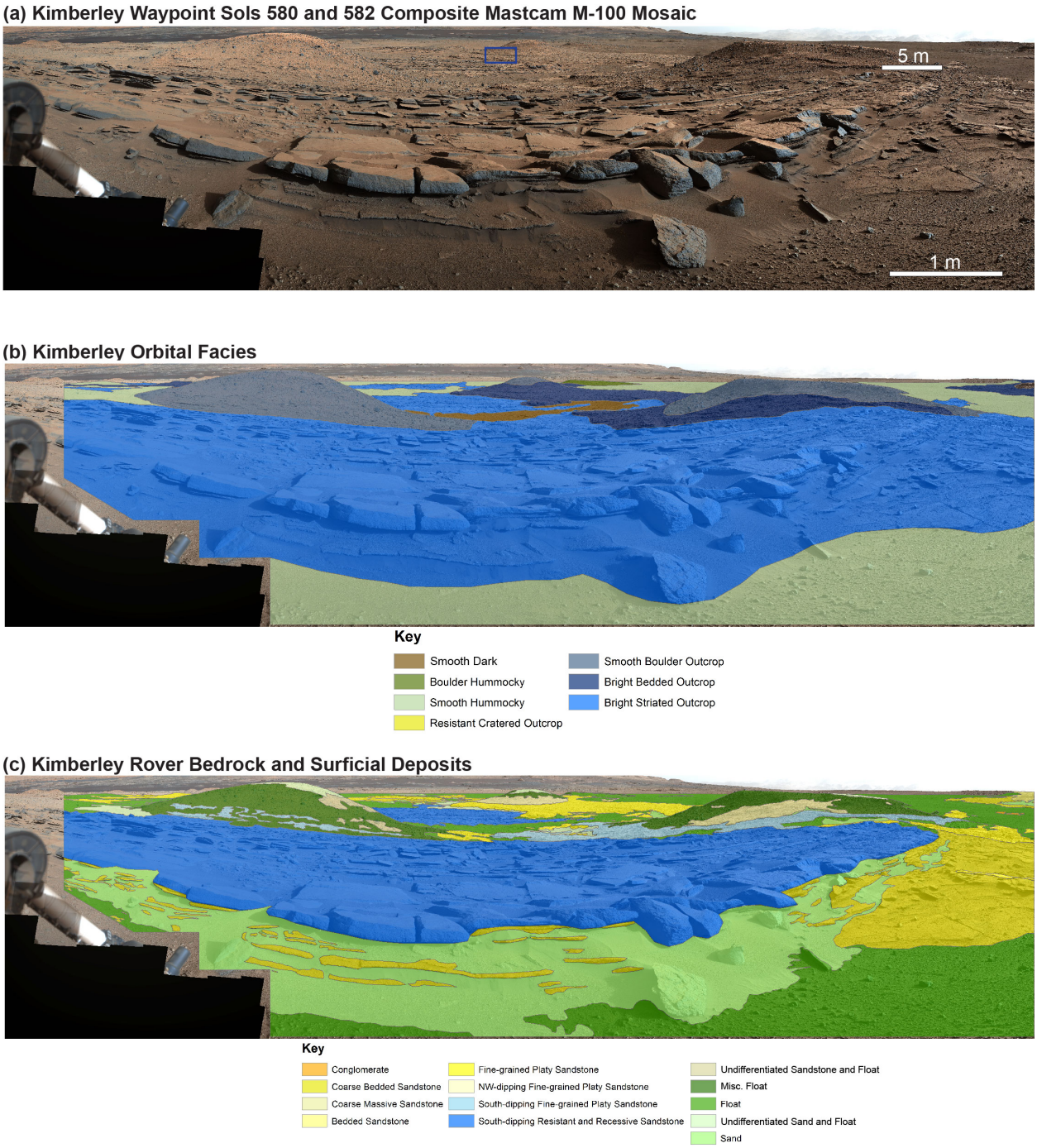

Figure 10. Rover mosaic of the Kimberley waypoint. (a) Sol 580 Mastcam M-100 Mosaic. Blue box shows the portion of the Kimberley outcrop examined with Curiosity's contact science instruments, (b) mosaic annotated with mapped orbital facies, (c) mosaic annotated with bedrock lithology and surficial deposit type observed in rover images.

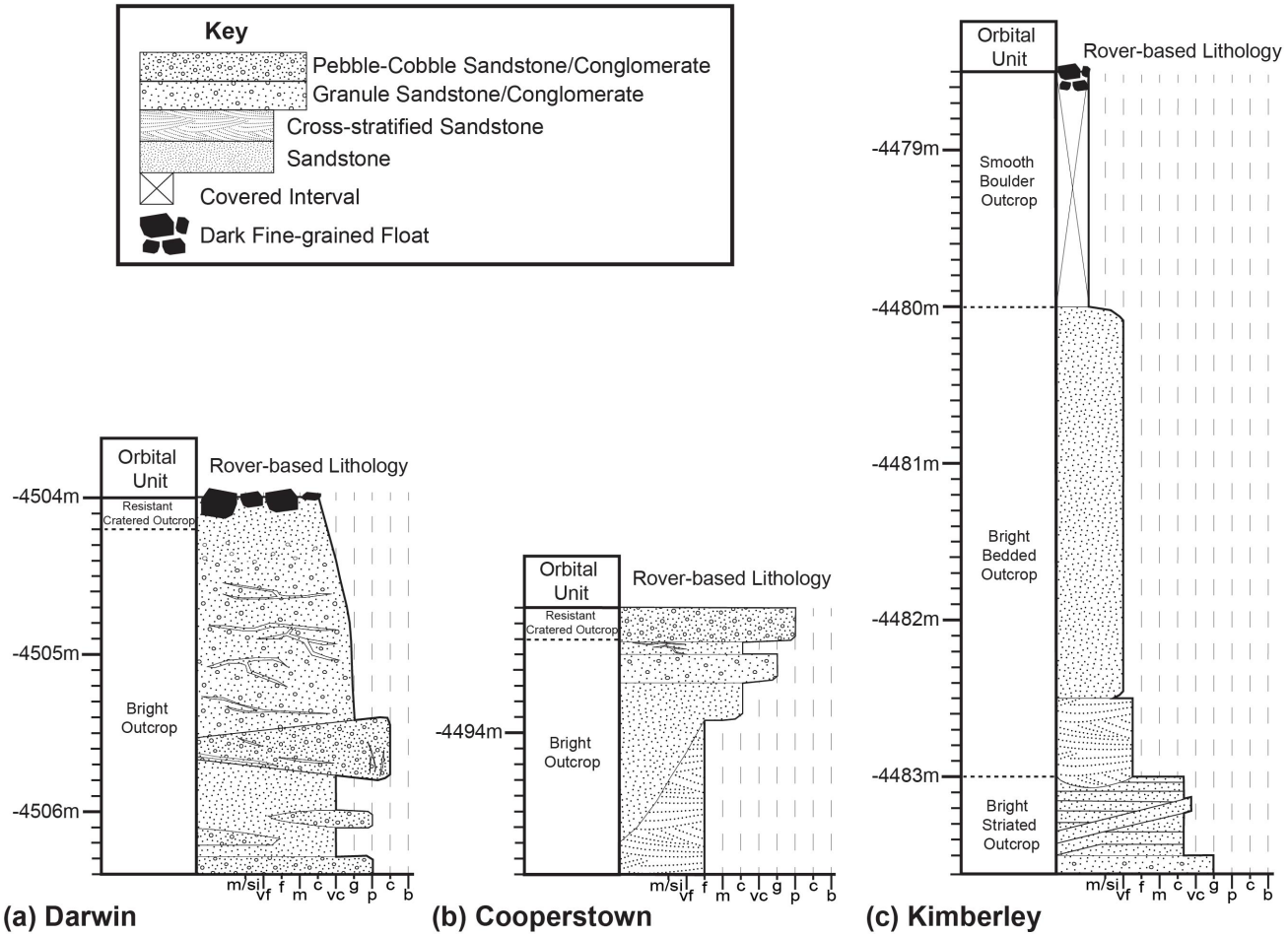

1028

1029 **Figure 11.** Stratigraphic columns showing mapped orbital facies interpreted as stratigraphic units compared with rover observations of

1030 bedrock lithology for (a) Darwin, (b) Cooperstown, (c) Kimberley.

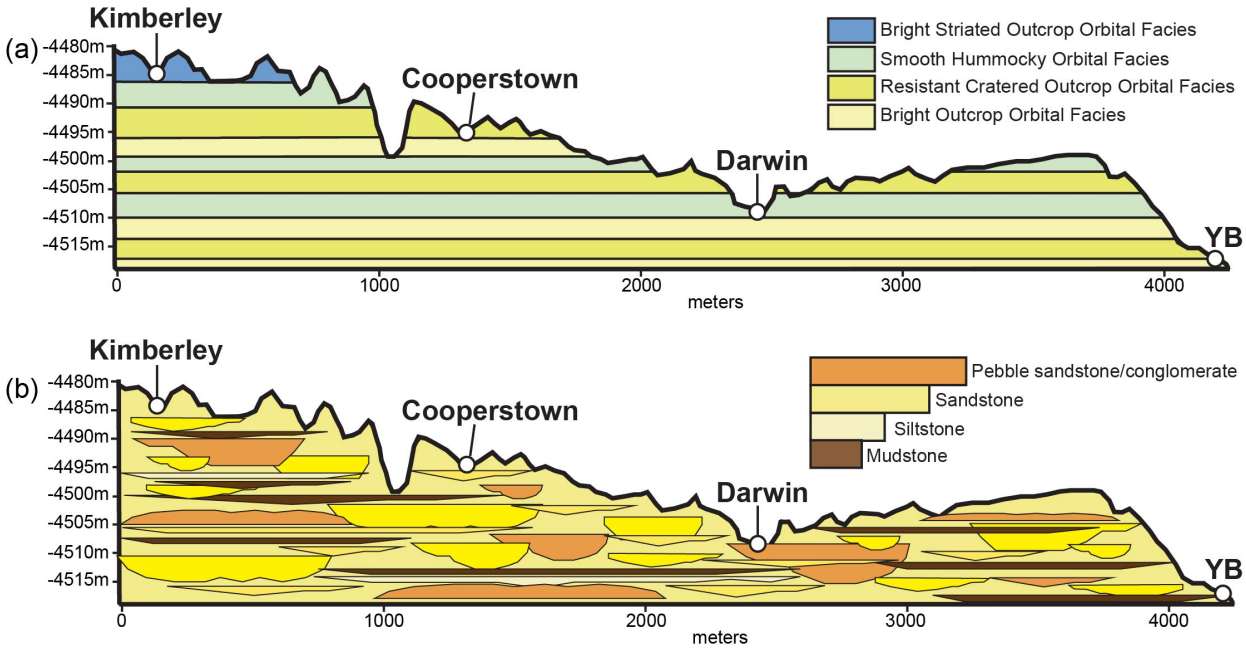

1031

1032 **Figure 12.** Schematic showing (a) Bradbury Rise stratigraphy interpretation derived from orbital

1033 mapping, and (b) the Bradbury Rise in situ fluvial/alluvial depositional interpretation.

1034